

Commerce, pollution, and solar energy yield gaps across Northeast Asia

Fei Yao,^{*,†,‡} Paul I. Palmer,^{†,‡} Jianzheng Liu,[¶] Hongwen Chen,[§] and Yuan
Wang^{||,⊥}

[†]*National Centre for Earth Observation, University of Edinburgh, Edinburgh, EH9 3FF,
UK*

[‡]*School of GeoSciences, University of Edinburgh, Edinburgh, EH9 3FF, UK*

[¶]*School of Public Affairs, Xiamen University, Xiamen, Fujian 361005, China*

[§]*School of Tourism, Nanchang University, Nanchang, Jiangxi 330031, China*

^{||}*Department of Architecture, National University of Singapore, Singapore 117566,
Singapore*

[⊥]*Asian School of the Environment and Earth Observatory of Singapore, Nanyang
Technological University, Singapore 639798, Singapore*

E-mail: Fei.Yao@ed.ac.uk

Abstract

Differences between the actual ability to generate solar energy from photovoltaic (PV) panels and the potential ability we denote as the solar energy yield gap (SEYG). We focus on the role of atmospheric particulate matter (PM) and PM deposited on PV panels, associated with domestic and international trade, in influencing SEYGS by attenuating the sunlight the panels receive. We quantify the source–receptor relationships of SEYGS across Northeast Asia (NEA), including China, South Korea, and Japan.

We estimate a SEYG of 33.6 TWh/yr due to the production of goods and services across NEA in 2019. In contrast, the SEYG linked to the consumption of goods and services is lower at 24.6 TWh/yr, with the 9 TWh/yr difference accounting for the net exports outside NEA. Imports have only avoided a SEYG of 1.4 TWh/yr across NEA. Addressing regional SEYGS requires a coordinated response from the producers and consumers of goods and services.

Main

Rapidly transitioning from conventional to renewable energy sources is key to addressing the linked challenges of air pollution and climate change, but it is increasingly recognized that air pollution and climate change affect the supply and demand of renewable energy.^{1–4} Whether we continue this vicious cycle or transform it into a virtuous cycle depends on the speed at which we transition away from carbon-based energy sources to meet growing energy needs of the world’s population.

In this study, we examine the impacts of particulate matter (PM) on the functioning of solar photovoltaic (PV) panels. Atmospheric PM significantly impacts solar energy generation by attenuating incoming light intercepted by the panels.⁵ PM can also be deposited onto the PV panels, which also attenuates the incoming solar energy needed to excite the electrons in the PV semiconductor material.^{6,7} Billions of dollars are lost every year in the solar energy industry due to these PM impacts.^{8,9} Previous studies have focused on mitigating the solar energy generation losses by reducing PM emissions from anthropogenic sectors,^{10–12} recognizing that controlling natural sources of PM are more difficult to control. These anthropogenic PM emissions originate from producers of goods and services that respond to changes in domestic and international consumer demands.¹³ This raises an important question about the extent to which domestic and international consumers should be responsible for the resulting solar energy generation losses in the producing country. Here,

we illustrate this challenge using trade across Northeast Asia (NEA) – China, South Korea, and Japan – that include some of the world's largest economies and have suffered significant environmental impacts¹⁴ partly associated with commerce.

To estimate and attribute the regional solar energy yield gap (SEYG) across NEA due to PM emissions, we integrate models that describe regional trade fluxes that can be translated in PM emissions;¹⁵ atmospheric chemistry and transport that describe how PM evolves in space and time;¹⁶ radiative transfer that describes how atmospheric and deposited PM attenuate incoming sunlight;^{7,11,17} and a solar PV performance model¹⁸ that describes how attenuated light from atmospheric and deposited PM affects SEYGS. We quantify SEYGS using the difference between actual and potential maximum values, if excluding PM impacts, based on the solar PV electricity generation. The solar PV electricity generation is determined by combining solar PV efficiency described by capacity factors (CFs) – defined as the ratio of a PV panel's actual power output to its maximum possible output^{7,8,11} – outputted from the integrated model with a satellite-derived solar PV installations data.¹⁹ We distinguish between the role of atmospheric and deposited PM, which we denote as PM dimming and soiling, respectively.

Our experimental design allows us to examine the: 1) geographical distribution of solar PV efficiency and how it is influenced by PM associated with trade; 2) country-level attribution of SEYGS across NEA due to domestic and international production and consumption of goods and services; and 3) sensitivity of the SEYG estimates and attributions to the cleaning of PV panels, either by rainfall or manual labour.

Solar PV efficiency and its modulation by PM associated with trade

Figure 1 shows solar PV efficiency and its losses (Δ CFs) due to PM dimming and soiling for flat, tilt, and one-axis tracking (OAT) panels across NEA, building on our previous work.¹¹ Compared to the flat panels, tilt panels show increased solar PV efficiency in northern high latitudes, and OAT panels show increased solar PV efficiency across the entire study

domain. In contrast, losses in solar PV efficiency due to PM dimming and soiling exhibit more consistent spatial patterns across the three types of panels, with the magnitude of losses increasing progressively from flat to tilted to OAT panels. PM dimming primarily affects northern and eastern China, China's Sichuan Basin, and over the eastern Indo-Gangetic Plain²⁰ including Bangladesh, while PM soiling mainly impacts the Gobi Desert. PM soiling in magnitude is comparable to PM dimming, except over the Gobi Desert, where it exceeds double the maximum PM dimming observed in eastern China (0.11 versus 0.05). Given the similar spatial patterns of solar PV efficiency losses due to PM pollution across the three types of panels, and their attribution (in work not shown) to domestic and international production and consumption of goods and services across NEA, we onwards focus on OAT panels for the discussion of the results. These panels offer superior performance and closely align with the satellite-derived solar PV installations data¹⁹ used in this work.

Figure 2 illustrates the grid-level attribution of solar PV efficiency losses in OAT panels to domestic and international production and consumption of goods and services across NEA. Generally, we find that PM emissions, irrespective of whether they are associated with the production or consumption of goods and services, lead to the largest reductions in solar PV efficiency in the country where the production or consumption occurs, with smaller impacts over the immediately adjacent countries. PM emissions from the production of goods and services in one country reduce solar PV efficiency in another country exclusively by atmospheric transport, while solar PV efficiency losses in one country due to PM emissions from the consumption of goods and services in another country are associated with atmospheric transport of PM and with international trade. Figure 2, along with Supplementary Figure 1, shows that losses in solar PV efficiency are smaller from a consumption- rather than a production-centric viewpoint, both for the three countries individually and for the upwind-downwind relationships among them, including those from China to South Korea and Japan, and from South Korea to Japan. An opposite pattern is observed for the "Others" category and for the downwind-upwind relationships among the three countries, including those from

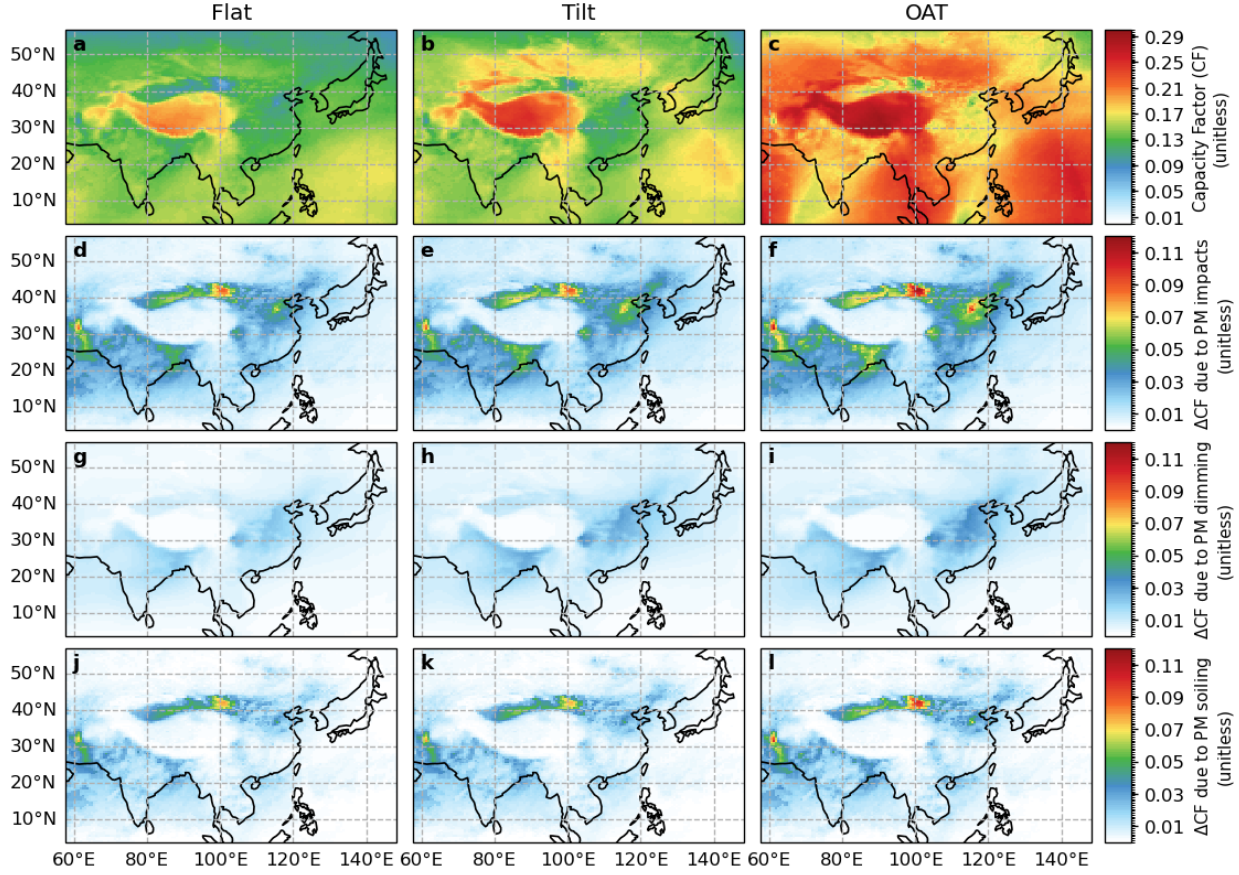


Figure 1: Geographical distribution of annual mean solar PV efficiency (**a,b,c**) described by capacity factors (CFs) and its losses (Δ CFs) due to PM pollution (**d,e,f**), including PM dimming (**g,h,i**) and soiling (**j,k,l**), for flat (**a,d,g,j**), tilt (**b,e,h,k**), and one-axis (**c,f,i,l**) tracking panels over Northeast Asia in 2015. Scales are different for the first and subsequent rows.

Japan to South Korea and China, and from South Korea to China. This contrast suggests narrower gaps in mutual contributions to solar PV efficiency losses from a consumption–rather than a production–centric perspective among China, South Korea, and Japan, which are all significantly influenced by the net exports of goods and services outside NEA. The differences between losses in solar PV efficiency due to PM dimming and soiling are generally small (Supplementary Figure 2), except over the Gobi Desert, where natural sources of PM result in significant levels of PM soiling that are not correlated with either the production or consumption of goods and services.

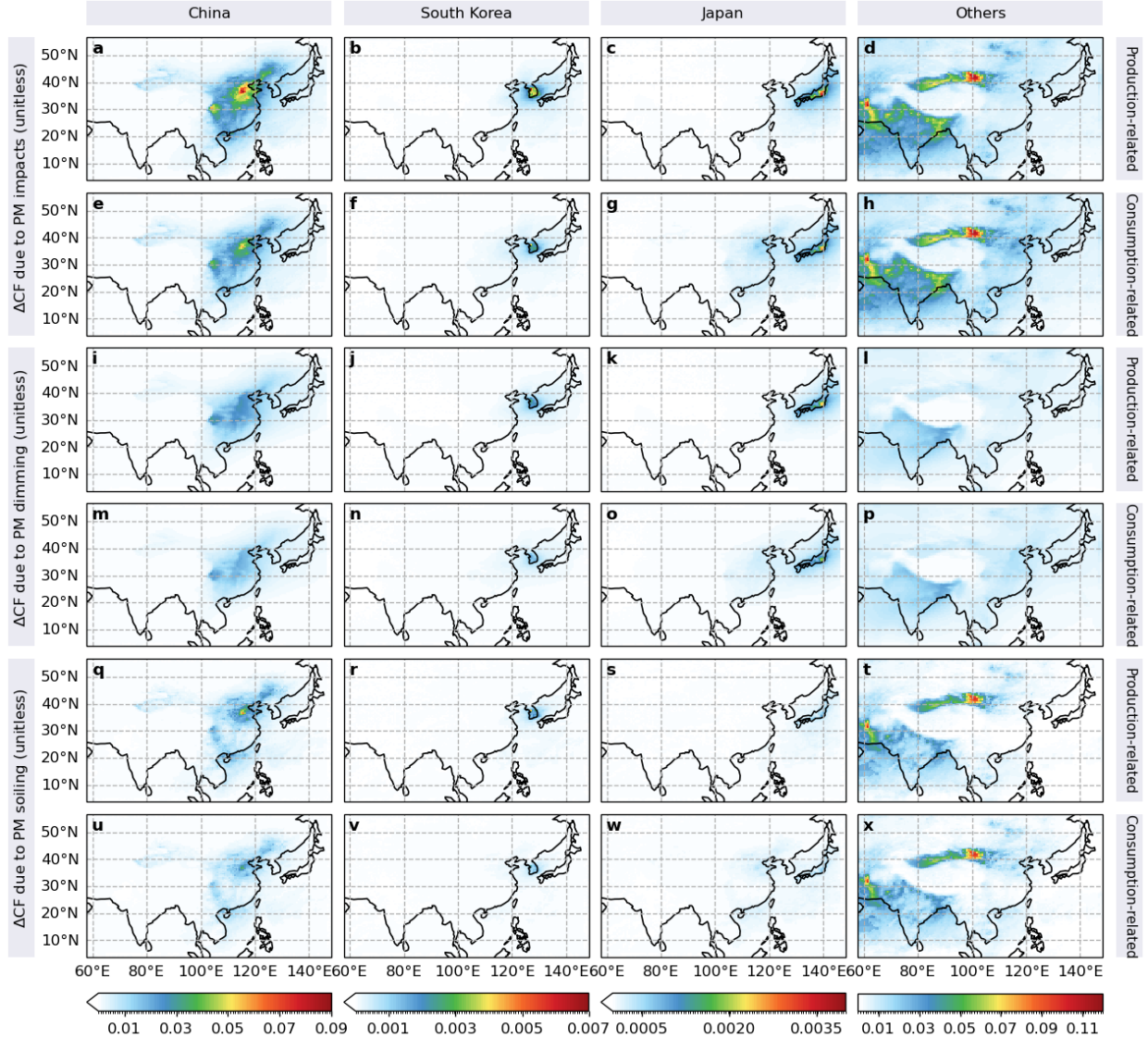


Figure 2: Geographical distribution of annual mean solar PV efficiency losses (ΔCFs) in OAT panels due to PM pollution (a-h), including PM dimming (i-p) and soiling (q-x), associated with emissions produced in (a-d,i-l,q-t) or induced by consumption (e-h,m-p,u-x) in China (a,e,i,m,q,u), South Korea (b,f,j,n,r,v), Japan (c,g,k,o,s,w), and "Others" (d,h,l,p,t,x) over Northeast Asia in 2015. Note that "Others" encompasses contributions from other countries and other natural sources of PM, but the latter cancels out when subtracting production-based results from consumption-based results, leaving only the contributions from net exports outside Northeast Asia. Scales are different for each column.

Attribution of PM-related SEYGs to the production and consumption of goods and services

Figure 3 shows a numerical breakdown of the country-level SEYG due to transboundary PM pollution in terms of the production and consumption of goods and services across NEA.

As we have seen in the analyses of solar PV efficiency losses, we find that consumption-based SEYG values are smaller than production-based values, both for the three countries individually and for the upwind-downwind relationships among them, including those from China to South Korea and Japan, and from South Korea to Japan. This is reflected by the negative differences shown in the diagonal and upper triangular parts of the heatmaps in Figure 3g-i. Conversely, a reversed pattern is observed for the "Others" category and for the downwind-upwind relationships among the three countries, including those from Japan to South Korea and China, and from South Korea to China. This is reflected by the positive differences shown in the lower triangular parts of the heatmaps in Figure 3g-i. The differences between the consumption-based and production-based SEYG values are statistically significant (Supplementary Figure 3), highlighting closer interdependence among China, South Korea, and Japan in their mutual contributions to solar PV efficiency losses from a consumption- rather than a production-centric standpoint, as well as the important role of net exports of goods and services outside NEA in determining the SEYG values across the region. Although we continue to observe similar contrasting patterns between PM dimming and soiling in consumption- and production-based SEYG values (Figure 3j,k), these patterns become slightly more noticeable as a result of aggregation. Nonetheless, our immediate focus is on reducing their combined impacts rather than addressing them individually.

Figure 3a-c further illustrates that China plays the largest role in determining production-based SEYGs in China, South Korea, and Japan (for PM soiling only). In contrast, Figure 3d-f reveals consumption-based SEYGs primarily driven by the "Others" category in these three countries. Additionally, China causes more production- than consumption-based SEYGs in NEA, whereas the opposite is true for South Korea, Japan, and the "Others" category. Of the total 33.6 TWh/yr SEYG in NEA resulting from the production of goods and services across the region, about 3.4% (1.1 TWh/yr) is related to the production of goods and services in a different NEA country from where the SEYG occurred. In contrast, of

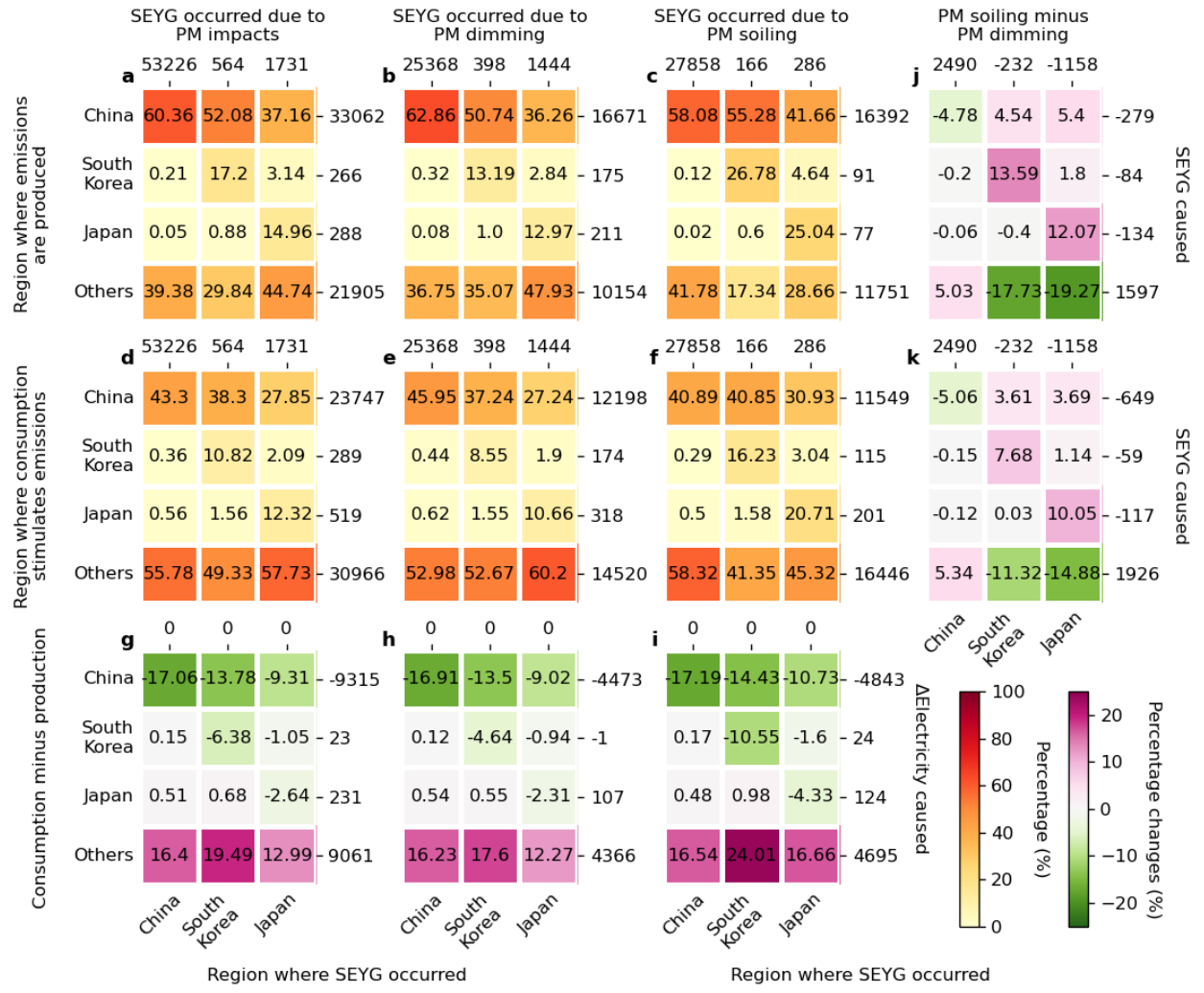


Figure 3: Contributions from source countries' production- (a-c) and consumption-related (d-f) emissions to receptor countries' solar energy energy yield gaps (SEYGs) attributable to PM pollution (a,d), including PM dimming (b,e) and soiling (c,f). Each cell in the grid shows the proportion of SEYGs that occurred in the country indicated by the column due to emissions produced in or induced by consumption in the country indicated by the row, wherein the consumption stimulates emissions domestically and elsewhere. The diagonal thus reflects the proportion of SEYGs in a country due to emissions produced in or induced by consumption within the same country. At the top, the total SEYGs (GWh/yr) occurred in each country are presented, while on the right, the total SEYGs (GWh/yr) in the three countries (aka Northeast Asia) caused by emissions produced in or induced by consumption in each country are outlined. Notably, the sum of the numbers at the top equals the sum at the right. g-i, Differences between consumption- and production-related results. j,k, Differences between PM soiling and dimming.

the total 24.6 TWh/yr SEYG in NEA due to consumption of goods and services across the region, about 5.0% (1.2 TWh/yr) is related to the consumption of goods and services in a different NEA country from where the SEYG occurred. All these findings indicate that,

when considering trade, the responsibility for SEYGs in NEA is more evenly distributed among China, South Korea, Japan, and other regions.

Figure 4 and our broader analysis (Supplementary Figures 4 – 6) result in the same conclusion: the SEYGs from PM dimming and soiling due to emissions produced in a country are primarily driven by consumption within that country, followed by consumption elsewhere. Of the total 33.6 TWh/yr SEYG across NEA due to PM dimming and soiling associated with emissions in NEA, about 23% (7.7 TWh/yr) is related to consumption outside NEA. When we break this regional estimate into country values we find for China, South Korea, and Japan that 23% (7.3 TWh/yr out of 32.3 TWh/yr), 25% (0.1 TWh/yr out of 0.4 TWh/yr), and 22% (0.21 TWh/yr out of 0.96 TWh/yr), respectively, can be attributed to consumption outside of NEA. Countries outside of NEA contributing to this consumption likely include the United States, the European Union (e.g., Germany), and other Asian countries (e.g., India) (Supplementary Figure 7), though we have not quantified their specific contributions.

The differences between SEYGs due to emissions linked to goods and services ultimately consumed in a country/region and those linked to goods and services produced in a country/region, as shown in Figure 3g-i, reflect the impact of net imports on a country/region's solar energy generation. Using the SEYGs associated with a country/region's exports, as illustrated in Figure 4, we can easily derive the SEYGs embodied in exports versus imports across NEA, which we summarise in Table 1. Overall, NEA acts primarily as a net exporter, with exports accounting for up to 7.7 TWh/yr of SEYGs in 2019, while imports only offset 1.4 TWh/yr of SEYGs in the same year.

PM–related SEYGs' attributions mostly insensitive to rainfall and panel cleaning practices

Previous work has highlighted the significant benefits of rainfall and panel cleaning practices in reducing SEYGs due to PM pollution.^{7,11} To investigate the potential impact of these mitigation strategies on the source–receptor relationships of SEYGs across NEA, we rerun

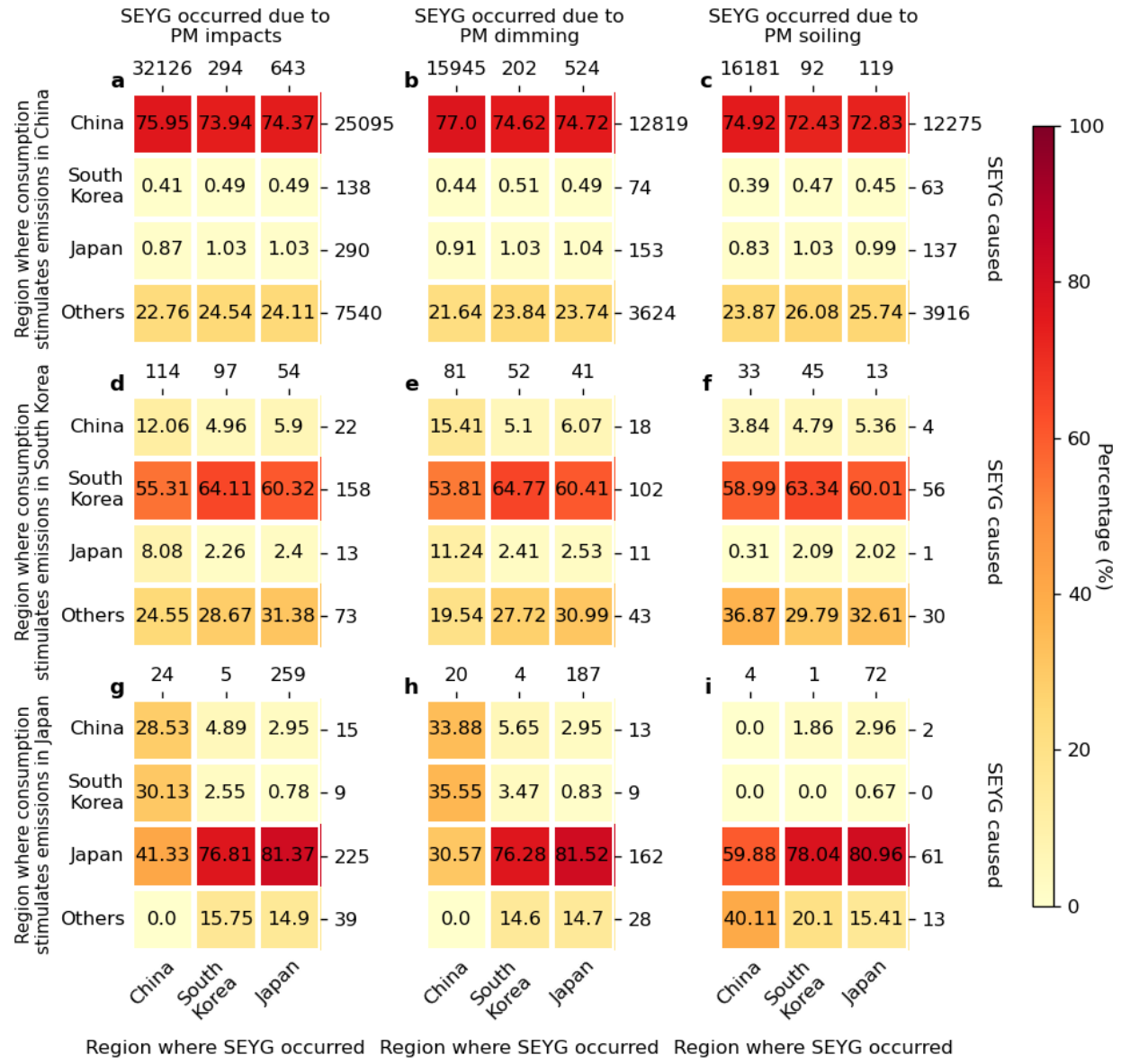


Figure 4: Contributions of production-related emissions from China (a-c), South Korea (d-f), and Japan (g-i) to solar energy yield gaps (SEYGs) in Northeast Asia due to PM pollution (a,d,g), including PM dimming (b,e,h) and soiling (c,f,i), further broken down to components linked to consumption in these countries and elsewhere. Each cell in the grid shows that proportion of SEYGs that occurred in the country indicated by the column due to emissions produced in a Northeast country that are induced by consumption in the country indicated by the row. The diagonal thus reflects the proportion of SEYGs in a country due to emissions produced in and induced by consumption within the same country. At the top, the total SEYGs (GWh/yr) occurred in each country due to emissions produced in a Northeast country are presented, while on the right, the total SEYGs (GWh/yr) in the three countries caused by emissions produced in a Northeast country that are induced by consumption in each country are outlined. Notably, the sum of the numbers at the top equals the sum at the right.

Table 1: Solar energy yield gaps (SEYGs, GWh yr⁻¹) embodied in imports versus exports across Northeast Asia in 2019. Net imports are derived by contrasting scenarios 5–7 with scenarios 2–4. Exports are derived using scenarios 8–16. Imports are derived as the sum of exports and net imports.

		China	South Korea	Japan	Northeast Asia
SEYGs due to PM pollution associated with	Exports	7726.23	34.82	48.26	7652.53
	Imports	-1350.71	-1.18	2.56	-1408.92
	Net imports	-9076.94	-36.00	-45.70	-9061.45
SEYGs due to PM dimming associated with	Exports	3667.56	18.48	34.60	3694.75
	Imports	-620.98	0.04	1.29	-671.73
	Net imports	-4288.54	-18.44	-33.31	-4366.48
SEYGs due to PM soiling associated with	Exports	4058.67	16.34	13.65	3959.39
	Imports	-729.73	-1.23	1.26	-735.59
	Net imports	-4788.41	-17.56	-12.39	-4694.98

all our calculations by excluding the role of rainfall and incorporating the panel cleaning practice, respectively, and compare the results with those from the baseline run described earlier. We expect based on previous work that these changes will affect mostly PM soiling. For brevity, we present only country-level results Supplementary Figures 8–11. We find that the rainfall and the frequency that panels are cleaned result in larger reductions in SEYGs, as expected. Nonetheless, we find differences between the sets of reruns and the baseline run are typically within $\pm 15\%$ for scenarios 2–7 and $\pm 5\%$ for scenarios 8–16. Consequently, the source–receptor relationships across NEA, determined by changes in meteorology, remain consistent with the baseline calculations. Similarly, the main conclusions reached from the baseline calculations remain unchanged.

Policy implications and concluding remarks

A wide range of environmental^{21–30} and social^{31–35} impacts embodied in trade have been assessed from a consumption perspective. Our work is the first to extend this perspective to include large SEYGs attributable to PM pollution. Our work is timely because of the rapid expansion of solar energy projects in the region to meet growing energy demands and to achieve carbon neutrality.

Our focus on SEYGs due to PM pollution shares concepts and methods with previous studies, particularly those examining PM-related health impacts. Balancing trade-offs and

synergies among different environmental and social impacts presents significant challenges for policymakers. Nonetheless, our and previous work can play a crucial role in timely evaluating and monitoring the effectiveness of existing policies and suggesting relevant modifications. These trade-related policies may include, but are not limited to: (1) adjustments of border taxes and tariffs, such as the European Union’s Carbon Border Adjustment Mechanism; (2) widening of technical and environmental standards to help reduce domestic and outsourced environmental impacts; (3) transfer of technology to help circumvent avoidable environmental impacts; and (4) interventions aimed at curbing unnecessary, unsustainable consumption.³⁶ These policies, by design, should help reduce SEYGs due to PM pollution, as well as other environmental and social impacts. However, the implementation of these and other policies should never be expected to be straightforward due to the many obstacles throughout. Our work, along with similar studies, can help policymakers navigate these obstacles by providing a comprehensive understanding of the environmental and social impacts of trade, including SEYGs due to PM pollution. Ultimately, we aim to maximise the benefits of trade, such as the employment opportunities generated, while minimising its negative impacts on the environment and society, achieving the decoupling of these impacts from economic growth.

Methods

We take four steps to estimate SEYGs due to transboundary PM pollution associated with trade across NEA (Supplementary Figure 12). First, we use a multi-regional input-output model¹⁵ to track the flow of goods and services among China, South Korea, and Japan, and thereby the associated emissions responsible for transboundary PM pollution. Second, we use the GEOS-Chem chemical transport model¹⁶ to simulate the PM levels in the atmosphere and on solar panels, the latter of which is further modulated by rainfall and panel cleaning practices. The built-in radiative transfer module in GEOS-Chem,¹⁷ alongside a custom

approach governing how solar radiation is reduced by PM accumulation on solar panels,^{7,11} allows us to estimate the final solar radiation that reaches the solar cells. Third, we use the PVLIB-Python model¹⁸ to estimate the solar PV efficiency of three widely used solar panel configurations: horizontal fixed (Flat), fixed with optimal tilt (Tilt), and one-axis tracking (OAT), though we primarily report results for OAT panels, as per reasons previously explained. Finally, we integrate the modelled solar PV efficiency with satellite-derived solar PV installation data¹⁹ to estimate the solar PV electricity generation and its losses (aka SEYGs) due to transboundary PM pollution associated with trade across NEA. We give detailed descriptions of these steps in the Supplementary Methods.

Our previous work¹¹ has extensively evaluated the performance of the integrated model against a range of *in situ* measurements of various PM-related variables, and we provide in the Supplementary Methods an additional evaluation of the model's performance in relation to ground measurements of the lumped PM_{2.5} (PM with an aerodynamic diameter $\leq 2.5 \mu\text{m}$) and its major chemical components, including sulfate, nitrate, ammonium, black carbon, and organic carbon, across NEA, reflecting updates in emission inputs. We find that the integrated model continues to perform reasonably well, though there remains some room for improvement. However, these areas for improvement do not impact the accuracy of quantifying source-receptor relationships for SEYGs across NEA in terms of self and mutual percentage contributions, as uncovered in this study.

We design a total of 16 major scenarios (Supplementary Table 1), each with three sub-scenarios (Supplementary Table 2), to attribute losses in solar PV efficiency (referred to as ΔCFs) and consequently, solar PV electricity generation (referred to as SEYGs) to trans-boundary PM pollution associated with trade across Northeast Asia. For each major scenario, its three subscenarios help isolate ΔCFs and SEYGs associated with PM dimming (e.g., $\Delta\text{CF}_{\text{Dimming}} = \text{CF}_{\text{NODimming}}^{\text{NOSoiling}} - \text{CF}_{\text{Dimming}}^{\text{NOSoiling}}$), soiling (e.g., $\Delta\text{CF}_{\text{Soiling}} = \text{CF}_{\text{Dimming}}^{\text{NOSoiling}} - \text{CF}_{\text{Dimming}}^{\text{Soiling}}$), and a combination of the two (e.g., $\Delta\text{CF}_{\text{Dimming+Soiling}} = \Delta\text{CF}_{\text{Dimming}} + \Delta\text{CF}_{\text{Soiling}} = \text{CF}_{\text{NODimming}}^{\text{NOSoiling}} - \text{CF}_{\text{Dimming}}^{\text{Soiling}}$). Using a zero-out approach,³⁷ scenarios 2–4 decom-

pose ΔCFs and SEYGs into components associated with emissions produced in China, South Korea, Japan, and elsewhere, e.g., $\Delta\text{CF}_{\text{Dimming+Soiling}}^{S1} = \Delta\text{CF}_{\text{Dimming+Soiling}}^{S1-S2} + \Delta\text{CF}_{\text{Dimming+Soiling}}^{S1-S3} + \Delta\text{CF}_{\text{Dimming+Soiling}}^{S1-S4} + \Delta\text{CF}_{\text{Dimming+Soiling}}^{\text{Remaining}}$. Similarly, scenarios 5–7 decompose ΔCFs and SEYGs into components associated with emissions induced by consumption in China, South Korea, Japan, and elsewhere, e.g., $\Delta\text{CF}_{\text{Dimming+Soiling}}^{S1} = \Delta\text{CF}_{\text{Dimming+Soiling}}^{S1-S5} + \Delta\text{CF}_{\text{Dimming+Soiling}}^{S1-S6} + \Delta\text{CF}_{\text{Dimming+Soiling}}^{S1-S7} + \Delta\text{CF}_{\text{Dimming+Soiling}}^{\text{Remaining}}$. Further, scenarios 8–10 decompose ΔCFs and SEYGs due to emissions produced in China into components associated with emissions induced by consumption in China, South Korea, Japan, and elsewhere, e.g., $\Delta\text{CF}_{\text{Dimming+Soiling}}^{S1-S2} = \Delta\text{CF}_{\text{Dimming+Soiling}}^{S1-S8} + \Delta\text{CF}_{\text{Dimming+Soiling}}^{S1-S9} + \Delta\text{CF}_{\text{Dimming+Soiling}}^{S1-S10} + \Delta\text{CF}_{\text{Dimming+Soiling}}^{\text{Remaining}}$. Likewise, scenarios 11–13 and 14–16 decompose ΔCFs and SEYGs due to emissions produced in South Korea and Japan, respectively, into components associated with emissions induced by consumption in China, South Korea, Japan, and elsewhere, e.g., $\Delta\text{CF}_{\text{Dimming+Soiling}}^{S1-S3} = \Delta\text{CF}_{\text{Dimming+Soiling}}^{S1-S11} + \Delta\text{CF}_{\text{Dimming+Soiling}}^{S1-S12} + \Delta\text{CF}_{\text{Dimming+Soiling}}^{S1-S13} + \Delta\text{CF}_{\text{Dimming+Soiling}}^{\text{Remaining}}$, and $\Delta\text{CF}_{\text{Dimming+Soiling}}^{S1-S4} = \Delta\text{CF}_{\text{Dimming+Soiling}}^{S1-S14} + \Delta\text{CF}_{\text{Dimming+Soiling}}^{S1-S15} + \Delta\text{CF}_{\text{Dimming+Soiling}}^{S1-S16} + \Delta\text{CF}_{\text{Dimming+Soiling}}^{\text{Remaining}}$. In short, scenarios 2–7 provide a comprehensive production- and consumption-based accounting of SEYGs due to transboundary PM pollution associated with trade across NEA. We also apply a two-tailed paired t-test to assess the statistical significance of the differences between these two sets of results. Additionally, scenarios 8–16 offer a detailed breakdown of the production-based SEYGs obtained in scenarios 2–4. By contrasting these with the consumption-based SEYGs from scenarios 5–7, we gain insights into the SEYGs associated with exports versus imports across NEA.

Acknowledgement

This research has been supported by the Natural Environment Research Council through the National Centre for Earth Observation: FY and PIP were supported by grant number #NE/R016518/1. The work of JL was supported by the National Natural Science Founda-

tion of China (Grant No. 42101199).

Author Contributions

The initial draft was prepared by FY, with review and editing by PIP. The modelling was performed by FY, with additional support from JL and HC. The formal analysis was conducted by FY, with further assistance from PIP, JL, and YW.

Supporting Information Available

The Supporting Information is available free of charge at XXX.

References

- (1) Song, Z.; Liu, J.; Yang, H. Air pollution and soiling implications for solar photovoltaic power generation: A comprehensive review. *Applied Energy* **2021**, *298*, 117247.
- (2) Gernaat, D. E.; de Boer, H. S.; Daioglou, V.; Yalew, S. G.; Müller, C.; van Vuuren, D. P. Climate change impacts on renewable energy supply. *Nature Climate Change* **2021**, *11*, 119–125.
- (3) Feron, S.; Cordero, R. R.; Damiani, A.; Jackson, R. B. Climate change extremes and photovoltaic power output. *Nature Sustainability* **2021**, *4*, 270–276.
- (4) Liu, L.; He, G.; Wu, M.; Liu, G.; Zhang, H.; Chen, Y.; Shen, J.; Li, S. Climate change impacts on planned supply–demand match in global wind and solar energy systems. *Nature Energy* **2023**, *8*, 870–880.
- (5) Li, X.; Wagner, F.; Peng, W.; Yang, J.; Mauzerall, D. L. Reduction of solar photovoltaic resources due to air pollution in China. *Proceedings of the National Academy of Sciences* **2017**, *114*, 11867–11872.

- (6) Bergin, M. H.; Ghoroi, C.; Dixit, D.; Schauer, J. J.; Shindell, D. T. Large reductions in solar energy production due to dust and particulate air pollution. *Environmental Science & Technology Letters* **2017**, *4*, 339–344.
- (7) Li, X.; Mauzerall, D. L.; Bergin, M. H. Global reduction of solar power generation efficiency due to aerosols and panel soiling. *Nature Sustainability* **2020**, *3*, 720–727.
- (8) Sweerts, B.; Pfenninger, S.; Yang, S.; Folini, D.; Van der Zwaan, B.; Wild, M. Estimation of losses in solar energy production from air pollution in China since 1960 using surface radiation data. *Nature Energy* **2019**, *4*, 657–663.
- (9) Ilse, K.; Micheli, L.; Figgis, B. W.; Lange, K.; Daßler, D.; Hanifi, H.; Wolfertstetter, F.; Naumann, V.; Hagendorf, C.; Gottschalg, R.; others Techno-economic assessment of soiling losses and mitigation strategies for solar power generation. *Joule* **2019**, *3*, 2303–2321.
- (10) Labordena, M.; Neubauer, D.; Folini, D.; Patt, A.; Lilliestam, J. Blue skies over China: The effect of pollution-control on solar power generation and revenues. *PloS one* **2018**, *13*, e0207028.
- (11) Yao, F.; Palmer, P. I. Source Sector Mitigation of Solar Energy Generation Losses Attributable to Particulate Matter Pollution. *Environmental Science & Technology* **2022**, *56*, 8619–8628.
- (12) Ghosh, S.; Dey, S.; Ganguly, D.; Roy, S. B.; Bali, K. Cleaner air would enhance Indias annual solar energy production by 6–28 TWh. *Environmental Research Letters* **2022**, *17*, 054007.
- (13) Meng, J.; Liu, J.; Xu, Y.; Guan, D.; Liu, Z.; Huang, Y.; Tao, S. Globalization and pollution: tele-connecting local primary PM_{2.5} emissions to global consumption. *Proceedings of the Royal Society A: Mathematical, Physical and Engineering Sciences* **2016**, *472*, 20160380.

- (14) Liu, J.; Li, J.; Yao, F. Source-receptor relationship of transboundary particulate matter pollution between China, South Korea and Japan: Approaches, current understanding and limitations. *Critical Reviews in Environmental Science and Technology* **2022**, *52*, 3896–3920.
- (15) Zhao, H.; Zhang, Q.; Guan, D.; Davis, S.; Liu, Z.; Huo, H.; Lin, J.; Liu, W.; He, K. Assessment of China's virtual air pollution transport embodied in trade by using a consumption-based emission inventory. *Atmospheric Chemistry and Physics* **2015**, *15*, 5443–5456.
- (16) Bey, I.; Jacob, D. J.; Yantosca, R. M.; Logan, J. A.; Field, B. D.; Fiore, A. M.; Li, Q.; Liu, H. Y.; Mickley, L. J.; Schultz, M. G. Global modeling of tropospheric chemistry with assimilated meteorology: Model description and evaluation. *Journal of Geophysical Research: Atmospheres* **2001**, *106*, 23073–23095.
- (17) Heald, C.; Ridley, D.; Kroll, J.; Barrett, S.; Cady-Pereira, K.; Alvarado, M.; Holmes, C. Contrasting the direct radiative effect and direct radiative forcing of aerosols. *Atmospheric Chemistry and Physics* **2014**, *14*, 5513–5527.
- (18) Holmgren, W. F.; Hansen, C. W.; Mikofski, M. A. Pvlib python: A python package for modeling solar energy systems. *Journal of Open Source Software* **2018**, *3*, 884.
- (19) Kruitwagen, L.; Story, K.; Friedrich, J.; Byers, L.; Skillman, S.; Hepburn, C. A global inventory of photovoltaic solar energy generating units. *Nature* **2021**, *598*, 604–610.
- (20) Mogno, C.; Palmer, P. I.; Knote, C.; Yao, F.; Wallington, T. J. Seasonal distribution and drivers of surface fine particulate matter and organic aerosol over the Indo-Gangetic Plain. *Atmospheric Chemistry and Physics* **2021**, *21*, 10881–10909.
- (21) Davis, S. J.; Caldeira, K. Consumption-based accounting of CO₂ emissions. *Proceedings of the national academy of sciences* **2010**, *107*, 5687–5692.

- (22) Davis, S. J.; Peters, G. P.; Caldeira, K. The supply chain of CO₂ emissions. *Proceedings of the National Academy of Sciences* **2011**, *108*, 18554–18559.
- (23) Lenzen, M.; Moran, D.; Kanemoto, K.; Foran, B.; Lobefaro, L.; Geschke, A. International trade drives biodiversity threats in developing nations. *Nature* **2012**, *486*, 109–112.
- (24) Oita, A.; Malik, A.; Kanemoto, K.; Geschke, A.; Nishijima, S.; Lenzen, M. Substantial nitrogen pollution embedded in international trade. *Nature Geoscience* **2016**, *9*, 111–115.
- (25) Lin, J.; Pan, D.; Davis, S. J.; Zhang, Q.; He, K.; Wang, C.; Streets, D. G.; Wuebbles, D. J.; Guan, D. Chinas international trade and air pollution in the United States. *Proceedings of the National Academy of Sciences* **2014**, *111*, 1736–1741.
- (26) Lin, J.; Tong, D.; Davis, S.; Ni, R.; Tan, X.; Pan, D.; Zhao, H.; Lu, Z.; Streets, D.; Feng, T.; others Global climate forcing of aerosols embodied in international trade. *Nature Geoscience* **2016**, *9*, 790–794.
- (27) Zhang, Q.; Jiang, X.; Tong, D.; Davis, S. J.; Zhao, H.; Geng, G.; Feng, T.; Zheng, B.; Lu, Z.; Streets, D. G.; others Transboundary health impacts of transported global air pollution and international trade. *Nature* **2017**, *543*, 705–709.
- (28) Dalin, C.; Wada, Y.; Kastner, T.; Puma, M. J. Groundwater depletion embedded in international food trade. *Nature* **2017**, *543*, 700–704.
- (29) Li, R.; Zhang, J.; Krebs, P. Global trade drives transboundary transfer of the health impacts of polycyclic aromatic hydrocarbon emissions. *Communications Earth & Environment* **2022**, *3*, 170.
- (30) Xing, Z.; Chang, R.; Song, Z.; Zhang, Y.; Muntean, M.; Feng, K.; Liu, Y.; Ma, Z.;

- Wang, J.; Zhang, J.; others International trade shapes global mercury–related health impacts. *PNAS nexus* **2023**, *2*, pgad128.
- (31) Alsamawi, A.; Murray, J.; Lenzen, M. The employment footprints of nations: uncovering master-servant relationships. *Journal of Industrial Ecology* **2014**, *18*, 59–70.
- (32) Simas, M. S.; Golsteijn, L.; Huijbregts, M. A.; Wood, R.; Hertwich, E. G. The Bad Labor footprint: quantifying the social impacts of globalization. *Sustainability* **2014**, *6*, 7514–7540.
- (33) Alsamawi, A.; McBain, D.; Murray, J.; Lenzen, M.; Wiebe, K. S.; Alsamawi, A.; McBain, D.; Murray, J.; Lenzen, M.; Wiebe, K. S. The inequality footprints of nations; A novel approach to quantitative accounting of income inequality. *The social footprints of global trade* **2017**, 69–91.
- (34) Xiao, Y.; Norris, C. B.; Lenzen, M.; Norris, G.; Murray, J. How social footprints of nations can assist in achieving the sustainable development goals. *Ecological Economics* **2017**, *135*, 55–65.
- (35) Xiao, Y.; Lenzen, M.; Benoît-Norris, C.; Norris, G. A.; Murray, J.; Malik, A. The corruption footprints of nations. *Journal of Industrial Ecology* **2018**, *22*, 68–78.
- (36) Wiedmann, T.; Lenzen, M. Environmental and social footprints of international trade. *Nature geoscience* **2018**, *11*, 314–321.
- (37) McDuffie, E. E.; Martin, R. V.; Spadaro, J. V.; Burnett, R.; Smith, S. J.; O'Rourke, P.; Hammer, M. S.; van Donkelaar, A.; Bindle, L.; Shah, V.; others Source sector and fuel contributions to ambient PM_{2.5} and attributable mortality across multiple spatial scales. *Nature communications* **2021**, *12*, 1–12.

Supporting Information for:

Commerce, pollution, and solar energy yield gaps

across Northeast Asia

Fei Yao,^{*,†,‡} Paul I. Palmer,^{†,‡} Jianzheng Liu,[¶] Hongwen Chen,[§] and Yuan Wang^{||,⊥}

[†]*National Centre for Earth Observation, University of Edinburgh, Edinburgh, EH9 3FF, UK*

[‡]*School of GeoSciences, University of Edinburgh, Edinburgh, EH9 3FF, UK*

[¶]*School of Public Affairs, Xiamen University, Xiamen, Fujian 361005, China*

[§]*School of Tourism, Nanchang University, Nanchang, Jiangxi 330031, China*

^{||}*Department of Architecture, National University of Singapore, Singapore 117566, Singapore*

[⊥]*Asian School of the Environment and Earth Observatory of Singapore, Nanyang Technological University, Singapore 639798, Singapore*

E-mail: Fei.Yao@ed.ac.uk

Table of Contents

Supplementary Methods	4
Multi-regional input-output model	4
GEOS-Chem chemical transport model with built-in radiative transfer module . .	8
Linking GEOS-Chem to the PVLIB-Python model	9
Linking the PVLIB-Python model to satellite-derived solar PV installations data	11
Model evaluation	13
Supplementary Tables	14
Supplementary Table 1	15
Supplementary Table 2	15
Supplementary Table 3	15
Supplementary Table 4	16
Supplementary Table 5	17
Supplementary Figures	18
Supplementary Figure 1	18
Supplementary Figure 2	18
Supplementary Figure 3	19
Supplementary Figure 4	20
Supplementary Figure 5	21
Supplementary Figure 6	22
Supplementary Figure 7	23
Supplementary Figure 8	24
Supplementary Figure 9	25
Supplementary Figure 10	26
Supplementary Figure 11	27
Supplementary Figure 12	28

Supplementary Figure 13	29
Supplementary Figure 14	30
Supplementary Figure 15	31
Supplementary Figure 16	32
Supplementary Figure 17	33
Supplementary Figure 18	34
Supplementary Figure 19	35
References	36

Supplementary Methods

Multi-regional input-output model

Our definition of production- and consumption-based emission inventories are consistent with the previous studies.¹⁻⁵ Production-based emission inventories are compiled based on the emissions produced within a region, regardless of where the goods and services are consumed. In contrast, consumption-based emission inventories are compiled based on the emissions produced to meet the consumption demands of a region, regardless of where the emissions are produced.

For production-based emission inventories, we use the Emissions Database for Global Atmospheric Research v5.0 (EDGARv5.0),⁶ of which the detailed disaggregation enables the follow-on multi-regional input-output (MRIO) analysis that generates the consumption-based emission inventories. We have also tried using EDGARv6.1,⁷ but it results in slightly poorer model performance compared to EDGARv5.0 (Model evaluation), likely because EDGARv5.0 has already taken into account the implementation of China's clean air actions in the year 2015, while there are only minor improvements over Northeast Asia (NEA) between these two versions. EDGARv8.1⁸ is not available at the time of our model simulations. We apply region- and sector- specific non-methane volatile organic compound (NMVOC) speciation profiles from the EDGARv4.3.2 database⁹ for the disaggregation of NMVOC emissions in EDGARv5.0 into 25 species for better model simulations. In contrast to previous studies,⁵ these NMVOC emissions can now be ascribed to particular sectors; thus, they are involved in constructing the follow-on consumption-based emission inventories and vary among different scenario runs. Ultimately, we obtain the production-based emission inventories for each month of the year 2015 at a spatial resolution of $0.1^\circ \times 0.1^\circ$, covering six species of air pollutants: sulfur dioxide (SO_2), nitrogen oxides (NO_x), carbon monoxide (CO), black carbon (BC), organic carbon (OC), and ammonia (NH_3), plus 25 NMVOC species.

For consumption-based emission inventories, we use the MRIO model to estimate the emissions produced in one region to meet the consumption demands of another region. The MRIO analysis is based on monetary flows between sectors across different regions:

$$\begin{bmatrix} \mathbf{x}^1 \\ \mathbf{x}^2 \\ \mathbf{x}^3 \\ \vdots \\ \mathbf{x}^m \end{bmatrix} = \begin{bmatrix} \mathbf{A}^{1,1} & \mathbf{A}^{1,2} & \mathbf{A}^{1,3} & \dots & \mathbf{A}^{1,m} \\ \mathbf{A}^{2,1} & \mathbf{A}^{2,2} & \mathbf{A}^{2,3} & \dots & \mathbf{A}^{2,m} \\ \mathbf{A}^{3,1} & \mathbf{A}^{3,2} & \mathbf{A}^{3,3} & \dots & \mathbf{A}^{3,m} \\ \vdots & \vdots & \vdots & \ddots & \vdots \\ \mathbf{A}^{m,1} & \mathbf{A}^{m,2} & \mathbf{A}^{m,3} & \dots & \mathbf{A}^{m,m} \end{bmatrix} \begin{bmatrix} \mathbf{x}^1 \\ \mathbf{x}^2 \\ \mathbf{x}^3 \\ \vdots \\ \mathbf{x}^m \end{bmatrix} + \begin{bmatrix} \sum_r \mathbf{y}^{1,r} \\ \sum_r \mathbf{y}^{2,r} \\ \sum_r \mathbf{y}^{3,r} \\ \vdots \\ \sum_r \mathbf{y}^{m,r} \end{bmatrix} = \begin{bmatrix} \sum_r \mathbf{A}^{1,r} \mathbf{x}^r \\ \sum_r \mathbf{A}^{2,r} \mathbf{x}^r \\ \sum_r \mathbf{A}^{3,r} \mathbf{x}^r \\ \vdots \\ \sum_r \mathbf{A}^{m,r} \mathbf{x}^r \end{bmatrix} + \begin{bmatrix} \sum_r \mathbf{y}^{1,r} \\ \sum_r \mathbf{y}^{2,r} \\ \sum_r \mathbf{y}^{3,r} \\ \vdots \\ \sum_r \mathbf{y}^{m,r} \end{bmatrix} \quad (1)$$

In matrix form, $\mathbf{x} = \mathbf{Ax} + \mathbf{y}$, where \mathbf{x}^c is a vector representing the total production (expressed as economic monetary output) of each sector in region c , which can be regarded as the sum of the intermediate demand $\sum_r \mathbf{A}^{c,r} \mathbf{x}^r$ plus the final demand $\sum_r \mathbf{y}^{c,r}$. For the former, $\mathbf{A}^{c,r}$ is a normalized matrix of intermediate consumption coefficients, where columns represent the input from sectors in region c required to produce one unit of output of each sector in region r . More specifically, $\mathbf{A}_{i,j}^{c,r}$ represents the input from sector i in region c required to produce one unit of output of sector j in region r . Therefore, $\mathbf{A}^{c,r} \mathbf{x}^r$ represents the total inputs needed from sectors in region c to meet the production demands of each sector in region r , and $\sum_r \mathbf{A}^{c,r} \mathbf{x}^r$ represents the total inputs needed from sectors in region c to meet the production demands of each sector in all regions. For the latter, $\mathbf{y}^{c,r}$ is a vector of each sector's output produced in region c and finally consumed in region r , and $\sum_r \mathbf{y}^{c,r}$ is a vector of each sector's output produced in region c and finally consumed in all regions.

Solving for the total output \mathbf{x} , Equation 1 can be rewritten as:

$$\mathbf{x} = (\mathbf{I} - \mathbf{A})^{-1} \mathbf{y}, \quad (2)$$

where \mathbf{I} is the identity matrix, and $(\mathbf{I} - \mathbf{A})^{-1}$ is the Leontief inverse matrix, which is useful

for deriving the fraction of region- and sector- specific production related to consumption in each and other regions by expanding Equation 2 to Equation 3:

$$\begin{aligned}
& \begin{bmatrix} x^1 \\ x^2 \\ x^3 \\ \vdots \\ x^m \end{bmatrix} = (\mathbf{I} - \mathbf{A})^{-1} \begin{bmatrix} \sum_r y^{1,r} \\ \sum_r y^{2,r} \\ \sum_r y^{3,r} \\ \vdots \\ \sum_r y^{m,r} \end{bmatrix} \\
& = (\mathbf{I} - \mathbf{A})^{-1} \begin{bmatrix} y^{1,1} + y^{1,2} + y^{1,3} + \cdots + y^{1,m} \\ y^{2,1} + y^{2,2} + y^{2,3} + \cdots + y^{2,m} \\ y^{3,1} + y^{3,2} + y^{3,3} + \cdots + y^{3,m} \\ \vdots \\ y^{m,1} + y^{m,2} + y^{m,3} + \cdots + y^{m,m} \end{bmatrix} \\
& = (\mathbf{I} - \mathbf{A})^{-1} \left(\begin{bmatrix} y^{1,1} \\ y^{2,1} \\ y^{3,1} \\ \vdots \\ y^{m,1} \end{bmatrix} + \begin{bmatrix} y^{1,2} \\ y^{2,2} \\ y^{3,2} \\ \vdots \\ y^{m,2} \end{bmatrix} + \begin{bmatrix} y^{1,3} \\ y^{2,3} \\ y^{3,3} \\ \vdots \\ y^{m,3} \end{bmatrix} + \cdots + \begin{bmatrix} y^{1,m} \\ y^{2,m} \\ y^{3,m} \\ \vdots \\ y^{m,m} \end{bmatrix} \right) \\
& = (\mathbf{I} - \mathbf{A})^{-1} \begin{bmatrix} y^{1,1} \\ y^{2,1} \\ y^{3,1} \\ \vdots \\ y^{m,1} \end{bmatrix} + (\mathbf{I} - \mathbf{A})^{-1} \begin{bmatrix} y^{1,2} \\ y^{2,2} \\ y^{3,2} \\ \vdots \\ y^{m,2} \end{bmatrix} + (\mathbf{I} - \mathbf{A})^{-1} \begin{bmatrix} y^{1,3} \\ y^{2,3} \\ y^{3,3} \\ \vdots \\ y^{m,3} \end{bmatrix} + \cdots + (\mathbf{I} - \mathbf{A})^{-1} \begin{bmatrix} y^{1,m} \\ y^{2,m} \\ y^{3,m} \\ \vdots \\ y^{m,m} \end{bmatrix}
\end{aligned}$$

$$= \begin{bmatrix} x_{\text{cons}}^{1,1} \\ x_{\text{cons}}^{2,1} \\ x_{\text{cons}}^{3,1} \\ \vdots \\ x_{\text{cons}}^{m,1} \end{bmatrix} + \begin{bmatrix} x_{\text{cons}}^{1,2} \\ x_{\text{cons}}^{2,2} \\ x_{\text{cons}}^{3,2} \\ \vdots \\ x_{\text{cons}}^{m,2} \end{bmatrix} + \begin{bmatrix} x_{\text{cons}}^{1,3} \\ x_{\text{cons}}^{2,3} \\ x_{\text{cons}}^{3,3} \\ \vdots \\ x_{\text{cons}}^{m,3} \end{bmatrix} + \cdots + \begin{bmatrix} x_{\text{cons}}^{1,m} \\ x_{\text{cons}}^{2,m} \\ x_{\text{cons}}^{3,m} \\ \vdots \\ x_{\text{cons}}^{m,m} \end{bmatrix}, \quad (3)$$

from which we denote $\mathbf{x}_{\text{cons}}^r = \begin{bmatrix} x_{\text{cons}}^{1,r} & x_{\text{cons}}^{2,r} & x_{\text{cons}}^{3,r} & \cdots & x_{\text{cons}}^{m,r} \end{bmatrix}^T$ as the production of each sector in each region related to the consumption in region r . $\mathbf{x}_{\text{cons}}^r$ is related to $\mathbf{y}^r = \begin{bmatrix} y^{1,r} & y^{2,r} & y^{3,r} & \cdots & y^{m,r} \end{bmatrix}^T$, which is the final consumption in region r that includes both the finished products in region r ($\mathbf{y}^{r,r}$) as well as those imported from other regions ($\mathbf{y}^{c,r}, c \neq r$), by the Leontief inverse matrix $(\mathbf{I} - \mathbf{A})^{-1}$, namely $\mathbf{x}_{\text{cons}}^r = (\mathbf{I} - \mathbf{A})^{-1} \mathbf{y}^r$. Thus, the fraction of region- and sector-specific production related to consumption in region r can be readily obtained as:

$$\mathbf{f}_{\text{cons}}^r = \frac{\mathbf{x}_{\text{cons}}^r}{\mathbf{x}} \quad (4)$$

Taking Beijing, China as an illustration, Supplementary Figure 7 shows its fraction of production in each sector linked to consumption within Beijing itself and in other regions. We ultimately calculate the region- and sector-specific emissions associated with consumption in region r ($\mathbf{E}_{\text{cons}}^r$) as:

$$\mathbf{E}_{\text{cons}}^r = \mathbf{f}_{\text{cons}}^r \odot \mathbf{E}, \quad (5)$$

where \mathbf{E} stands for the production-based emissions for each sector in each region, and \odot denotes the element-wise multiplication.

Our MRIO model has embedded the Chinese provincial MRIO table for 2015,¹⁰ which is obtained from Carbon Emission Accounts and Datasets, into the Organisation for Economic Co-operation and Development (OECD) Inter-Country Input-Output (ICIO) table

for 2015.¹¹ This results in a total of 31 Chinese provinces plus 64 other regions/countries, including South Korea and Japan. The definition for sectors vary among different MRIO tables as well as the EDGARv5.0 database, so we have harmonized them to the same 20 sectors through a mapping process (Supplementary Tables 3 – 4). In line with previous studies,⁵ household direct emissions from the residential sector are regarded as driven by domestic consumption. Therefore, we exclude them from this mapping process, keeping them constant across all scenario runs. Ultimately, we obtain the consumption–based emission inventories for 20 sectors in 95 regions for 2015. For the use in the integrated model, we distribute them to the monthly gridmaps using the same spatial proxies, temporal profiles, and NMVOC species segmentation as the production–based emissions, assuming that there are no distinctions in these aspects between production– and consumption–based emissions. Supplementary Figure 13 compares the grid–level production– and consumption–based emissions for species NO_x as an illustration. Compared to production–based emissions, which are confined to the borders of specific countries, consumption–based emissions are lower in magnitude but more widely distributed across the regions, reflecting the geographically more dispersed nature of the supply chain.

GEOS–Chem chemical transport model with built–in radiative transfer module

We use version 12.9.3 of the GEOS–Chem¹² tropshperic chemistry (aka 'tropchem') alongside a built-in radiative transfer module¹³ to provide 3–hourly output of PM levels and PM—attenuated versus PM–non–attenuated global horizontal irradiance (GHI) over NEA in 2015. Following half a year of model spin–up, we run the global model at a horizontal resolution of $2^\circ \times 2.5^\circ$ for all of 2015, from which we extract boundary conditions that we use to run the nested model over a regional domain of 5.5–55.0°N and 60.0–146.25°E (Supplementary Figure 14) at a finer horizontal resolution of $0.5^\circ \times 0.625^\circ$ also for all of 2015. All of our model simulations extend vertically through 47 terrain–following hybrid– σ levels from the

surface to 0.01 hPa, of which the first 30 layers lie below the dynamic tropause.

Model inputs used in this work are replicated from ref 14, except that we use EDGARv5.0 instead of EDGARv6.1 for our production–based emission inventories, as per the reasons explained above, and that we have six more scenarios for our consumption–based emission inventories. We turn off emissions that are shipped with the GEOS–Chem model but are already accounted for in our production– or consumption–based emission inventories to avoid double–counting. These include emissions from anthropogenic activities, agricultural soil NO_x , agricultural waste burning, aviation, and shipping. All of our model simulations are driven by the Modern–Era Retrospective analysis for Research and Applications, version 2 (MERRA–2) meteorological fields.¹⁵

Model outputs are replicated from ref 16. Briefly, we output PM–attenuated and PM–non–attenuated GHI, from which we estimate the direct normal irradiance (DNI) and the diffuse horizontal irradiance (DHI) using the Erbs model.¹⁷ We also output dry deposition velocities, dry mass concentrations, and thereby dry deposition fluxes of a total of 15 PM species: sulfate (SO_4^{2-}), nitrate (NO_3^-), ammonium (NH_4^+), hydrophilic (OCPI) and hydrophobic (OCPO) OC, secondary OC (SOC), hydrophilic and hydrophobic BC, and dust distributed in seven size bins. Sea salt is excluded from the PM soiling process due to the lack of measured optical properties when deposited on solar panels (Supplementary Table 5). Combining PM dry deposition fluxes with precipitation rates and elapsed time (relative to 00:00:00 UTC January 1, 2015) helps to determine the net accumulation of PM dry mass on solar panels, which ultimately determines the solar radiation received by solar cells, as detailed below.

Linking GEOS–Chem to the PVLIB–Python model

Our linking of GEOS–Chem to the PVLIB–Python model is detailed in a recent study¹⁶ so we briefly summarize it here. First, we derive from the aforementioned DNI, GHI, and DHI the beam (E_b), ground–reflected (E_g), and sky–diffuse (E_d) components of the irradiance

transposed to the solar panels, defined as "in" plane-of-array irradiance, $\text{POAI}_{in} = E_b + E_g + E_d$, by considering both solar positions and solar panel configurations.¹⁸ Second, we determine the net accumulation of PM dry mass and the associated broadband optical depth (τ) on solar panels, which will help derive the "out" plane-of-array irradiance (POAI_{out}) from POAI_{in} in the third step.

In mathematical terms, $\text{POAI}_{out} = \text{POAI}_{in} \times e^{-\tau}$, where $\tau = \sum_{i=1}^{15} ((E_{abs,i} + \beta_i E_{scat,i}) \times (\text{PM}_i^{Accum} - \text{PM}_i^{Removal}))$. Here, $E_{abs,i}$ and $E_{scat,i}$ are the absorption and scattering mass extinction coefficients of PM species i , respectively, β_i is the backscattering ratio of PM species i . The values for these three parameters are taken from refs 19,20 and are reproduced in Supplementary Table 5. The PM dry mass accumulation on solar panels, PM_i^{Accum} , is given by $\int_t (V_i^g \cos(\theta_T) + V_i^t) C_i dt$, where V_i^g and V_i^t are the gravitational and turbulent settling velocities of PM species i , respectively, C_i is the surface PM dry mass concentration of PM species i , and θ_T is the tilt angle of the solar panels. The PM dry mass removal from solar panels, $\text{PM}_i^{Removal}$, is a function of precipitation rates, p , and PM properties:^{16,20}

$$\text{PM}_i^{Removal} = \begin{cases} \text{PM}_i^{Accum}, & \text{if } p > 5 \text{ mm h}^{-1} \\ \left\{ \begin{array}{ll} \text{PM}_i^{Accum}, & \text{if } \text{PM}_i \in [\text{SO}_4^{2-}, \text{NO}_3^-, \text{NH}_4^+] \\ 0.5\text{PM}_i^{Accum}, & \text{otherwise} \end{array} \right., & \text{elif } 3 < p \leq 5 \text{ mm h}^{-1} \\ \left\{ \begin{array}{ll} \text{PM}_i^{Accum}, & \text{if } \text{PM}_i \in [\text{SO}_4^{2-}, \text{NO}_3^-, \text{NH}_4^+] \\ 0.5\text{PM}_i^{Accum}, & \text{elif } \text{PM}_i \in [\text{OCPI}, \text{OCPO}, \text{SOC}], \text{ elif } 1 < p \leq 3 \text{ mm h}^{-1} \\ 0, & \text{otherwise} \end{array} \right. & \text{otherwise} \end{cases} \quad (6)$$

We use version 0.8.0 of the PVLIB-Python model²¹ to take in the POAI_{out} as well as ambient temperature and wind speed from MERRA-2 to calculate the solar PV efficiency

of three widely used solar panel configurations: horizontal fixed (Flat), fixed with optimal tilt (Tilt), and one-axis tracking (OAT), though we primarily report results for OAT panels, as per reasons explained in the main text. As shown in Supplementary Figure 12, throughout this process, the cell temperature, effective radiance, direct current (DC) power, and alternating current (AC) power are sequentially calculated with a temperature model, a PV module¹, and an inverter². The capacity factors (CFs) are ultimately derived by dividing the AC power by AC power rating of the inverter. We consider a PV cell efficiency of 12.94% from solar energy to DC power and an inverter efficiency of 96% from DC power to AC power. Similar to refs 16,20,22, we have developed a wrapper for the PVLIB-Python model to facilitate its parallel computations for a large number of grids and time steps over NEA.

Linking the PVLIB-Python model to satellite-derived solar PV installations data

Our recent study¹⁶ combines the modelled Δ CFs with several bottom-up datasets of solar PV installations to illustrate the considerable rewards for the solar energy industry in East and South Asia from deep cuts in residential emissions. However, the bottom-up solar PV installations used in the study were only available at the provincial level, which limits the accuracy of our analysis. Leveraging a newly released global top-down inventory of commercial-, industrial-, and utility-scale solar PV installations,²³ we provide an improved estimate of solar energy yield gaps (SEYGs) by combining this facility-level dataset with our modelled Δ CFs within a geographic information system (GIS) program. We refer our readers to ref 23 for more details on this facility-level dataset of solar PV installations extracted from satellite imagery using machine learning. Briefly, for installations over 10,000 m² (approximately 600 kW), the authors achieved a precision of 98.6% and a modest trade-

¹Canadian_Solar_CS5P_220M____2009_

²ABB__MICRO_0_25_I_OUTD_US_208__208V_

off in recall at 90% relative to their test set – sufficient for the application in our work. For all detected and verified solar PV installations, the authors also provide estimates of their nominal capacities (P_{nom}). Supplementary Figure 15 shows the distribution of these solar PV installations over NEA.

Δ CFs simply refers to those CFs that are reduced by atmospheric and/or deposited PM, and they may be further decomposed into different components associated with production–versus consumption–based emissions. We extract the facility–level area–weighted Δ CFs from the grid–level Δ CFs within a GIS program. For each facility, we extract Δ CFs in grid cells within that facility’s boundary. For grid cells overlapping with more than one facility, we split them along the facility boundaries. With these complete (and split) grid cells and the associated areas and Δ CFs, we derive the corresponding area–weighted Δ CFs for each facility. We finally combine these facility–wise area–weighted Δ CFs with the nominal capacities of the facilities to estimate their SEYGs due to transboundary PM pollution over a period of time, say a year, as $SEYGs = \int_t \Delta CF(t) \times P_{nom}(t) dt$, where t is the time within a year.

The total SEYGs in a region of interest is simply the sum of all its facilities’ SEYGs, $\sum_{facilities} SEYGs$. Note, however, that there is a time mismatch between our modelled Δ CFs and the satellite–derived solar PV installations data, which are for the years 2015 and 2016–2018, respectively. In a balanced manner, we use all the detected and verified facilities for the calculation of SEYGs and $\sum_{facilities} SEYGs$, emphasizing that this is intended as an illustrative yet meaningful demonstration for possible cases in the year 2019. This approach is also justified by the difficulty of precisely knowing how each solar panel is managed in practice, such as cleaning practices that may affect Δ CFs and consequently SEYGs. Since the satellite–derived solar PV installations are for commercial–, industrial–, and utility–scale facilities, we follow previous studies^{16,24} to combine them with our modelled Δ CFs of OAT panels for the calculation of SEYGs. We acknowledge that this approach likely underestimates the actual SEYGs due to the lack of consideration of distributed solar PV installations. However, this issue cannot be easily addressed until a census of distributed

solar PV installations becomes available for NEA.

Model evaluation

We present an extended model evaluation against measured ground-level concentrations of the lumped PM_{2.5} and its major chemical components, including sulfate (SO₄²⁻), nitrate (NO₃⁻), ammonium (NH₄⁺), organic carbon (OC), and black carbon (BC) across NEA. We refer our readers to section 2.2 of ref 14 for details on the collection and quality control of these measurements from multiple sources. After performing data quality checks, the measurements for the lumped PM_{2.5} are averaged into monthly means and aggregated to the GEOS-Chem nested model grids. This facilitates an effective match and fair comparison with the simulated data, where modelled PM_{2.5} and its major chemical components are calculated in a way consistent with measurements: a relative humidity of 50%, temperature of 298 K, and a pressure of 1013.25 hPa.²⁵ For the measurements of the major chemical components of PM_{2.5}, the representative periods can vary from several days to months. Therefore, we sample our model values according to the locations and periods of these measurements to ensure a fair comparison.

As in ref 16, we describe the comparisons between model simulations and *in situ* measurements using the Pearson correlation coefficients (R), normalised mean bias (NMB), and normalised root mean squared error ($NRMSE$). The formulas are as follows:

$$R = \frac{\sum_{i=1}^N (M_i - \bar{M})(O_i - \bar{O})}{\sqrt{\sum_{i=1}^N (M_i - \bar{M})^2} \sqrt{\sum_{i=1}^N (O_i - \bar{O})^2}} \quad (7)$$

$$NMB = \frac{\sum_{i=1}^N (M_i - O_i)}{\sum_{i=1}^N O_i} \times 100\% \quad (8)$$

$$NRMSE = \frac{\sqrt{\frac{1}{N} \sum_{i=1}^N (M_i - O_i)^2}}{O_{\max} - O_{\min}}, \quad (9)$$

where M and O denote the model and measured values, respectively, with their mean values

denoted by \overline{M} and \overline{O} . O_{\max} and O_{\min} represent the maximum and minimum measured values, respectively, and N is the number of comparison data points.

Supplementary Figure 16 presents the overall model evaluation results, showing that the R , NMB , and $NRMSE$ between model and measured values range from 0.48 to 0.69, from 13.9% to 28.2%, and from 16.9% to 23.7% for different species, respectively. Notably, we initially observed poor model performance for black carbon (Supplementary Figure 17). We address this issue by re-distributing its emissions in EDGARv5.0 according to the spatial profile of the equivalent in the MIX Asian emission inventory,²⁶ which better represents regional characteristics. For the lumped $PM_{2.5}$, these values are 0.63, 41.3%, and 17%, respectively. Notably, all R values are statistically significant ($p < 0.001$), suggesting that the model effectively captures the variations of $PM_{2.5}$ and its major chemical components in Asia for the year 2015. Admittedly, the NMB is slightly high for the lumped $PM_{2.5}$. Nonetheless, this is a widespread occurrence across the majority of China, which overlaps with the majority of solar PV installations, as well as throughout South Korea and Japan (Supplementary Figure 18). This suggests a robust source–receptor relationship regarding SEYGs due to PM pollution associated with trade across NEA in terms of self and mutual percentage contributions, as revealed in our work. Even though the absolute values might be consistently high, this issue is partly counterbalanced by our exclusion of distributed solar panels in the calculation of SEYGs. As mentioned in the main text, we have also attempted to use EDGARv6.1. However, this resulted in slightly poorer model performance compared to EDGARv5.0 (Supplementary Figure 16 versus Supplementary Figure 19).

Overall, the above statistics indicate that the model performs reasonably well in simulating both the lumped and speciated $PM_{2.5}$, although there remains room for improvement, particularly regarding the R values of sulfate and black carbon, as well as the NMB values of the lumped $PM_{2.5}$. Despite these areas of improvement, the model’s performance validates its use in quantifying the source–receptor relationship of SEYGs due to PM pollution associated with trade among China, South Korea, and Japan.

Supplementary Tables

Supplementary Table 1: Design of experiments: Major scenarios.

Scenarios	Descriptions
S1	Baseline scenario with EDGARv5.0 emissions
S2	Exclude emissions produced in China in response to consumer demand worldwide
S3	Exclude emissions produced in South Korea in response to consumer demand worldwide
S4	Exclude emissions produced in Japan in response to consumer demand worldwide
S5	Exclude emissions induced by consumption in China, regardless of where they occur worldwide
S6	Exclude emissions induced by consumption in South Korea, regardless of where they occur worldwide
S7	Exclude emissions induced by consumption in Japan, regardless of where they occur worldwide
S8	Exclude emissions produced in China and induced by its own consumption
S9	Exclude emissions produced in China but induced by consumption in South Korea
S10	Exclude emissions produced in China but induced by consumption in Japan
S11	Exclude emissions produced in South Korea but induced by consumption in China
S12	Exclude emissions produced in South Korea and induced by its own consumption
S13	Exclude emissions produced in South Korea but induced by consumption in Japan
S14	Exclude emissions produced in Japan but induced by consumption in China
S15	Exclude emissions produced in Japan but induced by consumption in South Korea
S16	Exclude emissions produced in Japan and induced by its own consumption

Supplementary Table 2: Design of experiments: Subscenarios.

CF	Include PM dimming?	Include PM soiling?
CF ^{Soiling} <i>Dimming</i>	Yes	Yes
CF ^{NoSoiling} <i>Dimming</i>	Yes	No
CF ^{NoSoiling} <i>NO Dimming</i>	No	No

Supplementary Table 3: Harmonising the sectors of goods and services in the Chinese provincial MRIO table and the OECD ICIO table.

The embedded MRIO table	Chinese provincial MRIO table	OECD ICIO table
Agriculture	Agriculture, forestry and fishery products	Agriculture, forestry and fishing
Mining	Coal mining and processing products Oil and gas mining products Metal mining and processing products Non-metallic minerals	Mining and extraction of energy producing products Mining and quarrying of non-energy producing products Mining support service activities
Food and tobacco	Food and tobacco	Food products, beverages and tobacco
Textiles and Clothes	Textile Textile clothing, shoes, hats, leather	Textiles, wearing apparel, leather and related products
Wood and furniture	Wood products and furniture	Wood and products of wood and cork
Paper printing	Paper making, printing, cultural, educational and sports goods	Paper products and printing
Coke and petroleum	Petroleum, coking products and nuclear fuel processing products	Coke and refined petroleum products
Chemicals	Chemical products	Chemicals and pharmaceutical products Rubber and plastic products

Continued on next page

The embedded MRIO table	Chinese provincial MRIO table	OECD ICIO table
Non-metallic mineral	Non-metallic mineral products	Other non-metallic mineral products
Metals	Metal smelting products	Basic metals
	Metal products	Fabricated metal products
General equipment	General equipment, special equipment	Machinery and equipment, n.e.c.
Electrical and optical equipment	Electrical machinery and equipment	Computer, electronic and optical products
	Communication equipment, computers and other electronic equipment	Electrical equipment
	Instruments and meters	
Transport equipment	Transportation equipment	Motor vehicles, trailers and semi-trailers
		Other transport equipment
Other manufacturing	Other manufacturing products	Other manufacturing; repair and installation of machinery and equipment
	Scrap	
	Metal products, equipment repair services	
Electricity	Production and supply of electricity	Electricity, gas, water supply, sewerage, waste and remediation services
	Production and supply of heat and gas	
	Production and supply of water	
Construction	Construction	Construction
Wholesale and retail trade	Wholesale and retail	Wholesale and retail trade; repair of motor vehicles
Hotels and restaurants	Accommodation and catering	Accommodation and food services
Transport, postage, and warehousing	Transportation, warehousing and post	Transportation and storage
Other services	Others	Telecommunications Publishing, audiovisual and broadcasting activities IT and other information services Financial and insurance activities Real estate activities Other business sector services Public administration and defence; compulsory social security Education Human health and social work Arts, entertainment, recreation and other service activities Private households with employed persons

Supplementary Table 4: Harmonising the sectors of the embedded MRIO table and the EDGARv5.0 database.

The embedded MRIO table	EDGARv5.0
Agriculture	Manure management Rice cultivation Direct soil emissions Manure in pasture/range/paddock Other direct soil emissions Agricultural waste burning
Mining	Fugitive emissions from solid fuels Fugitive emissions from oil and gas Fossil fuel fires Fugitive emissions from gaseous fuels Fugitive emissions from liquid fuels
Food and tobacco	Production of pulp/paper/food/drink
Textiles and Clothes	Manufacturing Industries and Construction
Wood and furniture	Manufacturing Industries and Construction
Paper printing	Production of pulp/paper/food/drink

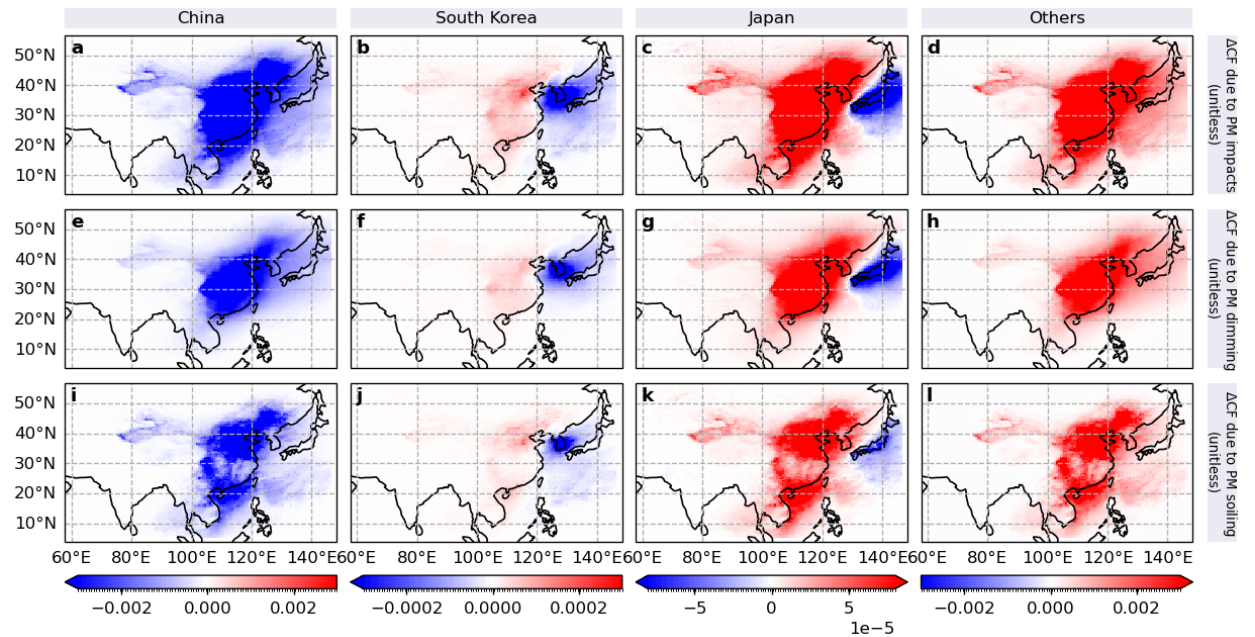
Continued on next page

The embedded MRIO table	EDGARv5.0	
Coke and petroleum	Other Energy Industries	
Chemicals	Soda ash production and use Production of chemicals Solvent and other product use: degrease Solvent and other product use: other Solvent and other product use: paint Solvent and other product use: chemicals	
Non-metallic mineral	Cement production Lime production Production of other minerals	
Metals	Production of metals	
General equipment	Manufacturing Industries and Construction	
Electrical and optical equipment	Semiconductor/electronics manufacture Electrical equipment	
Transport equipment	Manufacturing Industries and Construction	
Other manufacturing	Solid waste disposal on land Waste incineration Wastewater handling Other waste handling	
Electricity	Public electricity and heat production	
Construction	Manufacturing Industries and Construction	
Transport, postage, and warehousing	Domestic aviation Road transportation no resuspension Road transportation resuspension Rail transportation Inland navigation Other transportation	
Wholesale and retail trade	Residential (excluding household direct emissions) and other sectors	
Hotels and restaurants		
Other services		

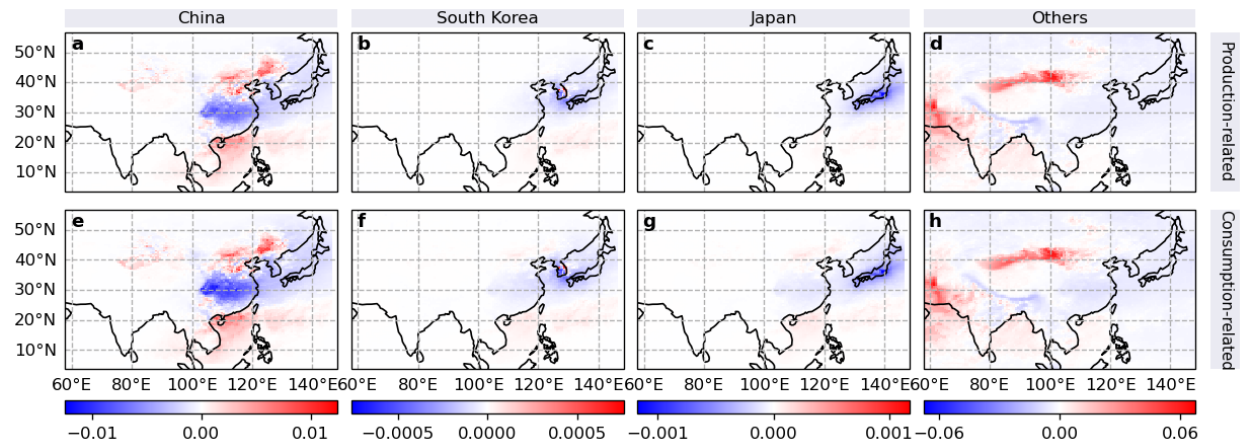
Supplementary Table 5: The measured optical properties of deposited PM taken from refs 19,20 used in this study.

Species	E_{abs} (m^2g^{-1})	β	E_{scat} (m^2g^{-1})
Dust	0.02	0.02	1.00
Organic carbon	0.00	0.30	4.00
Black carbon	8.00	0.30	0.00
Sulfate-nitrate-ammonium	0.00	0.30	4.00

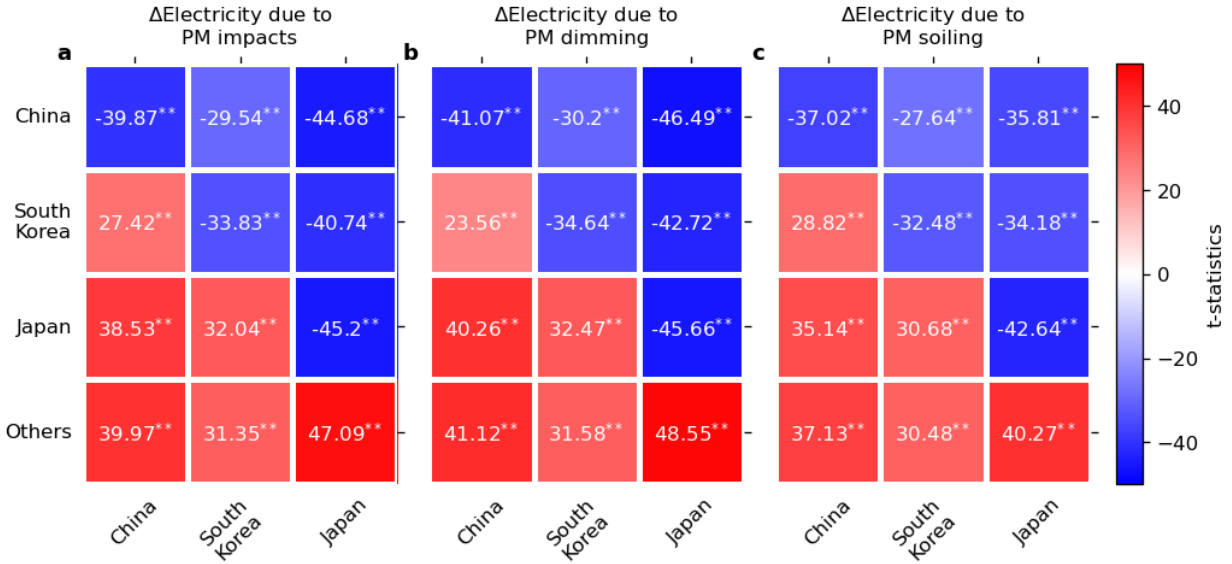
Supplementary Figures



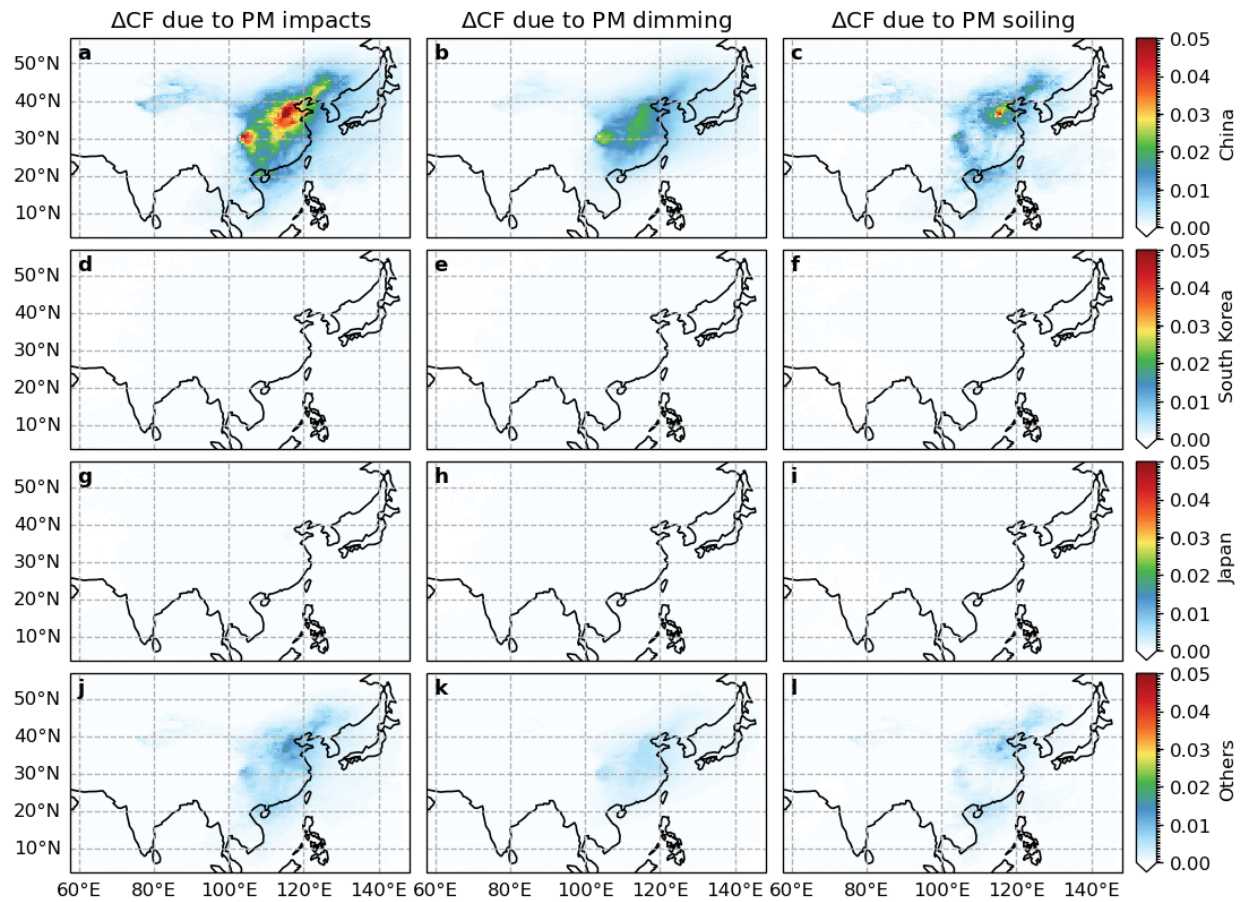
Supplementary Figure 1: The differences in annual mean losses of PV efficiency (Δ CFs) due to PM pollution (a-d), including PM dimming (e-h) and soiling (i-l), associated with emissions induced by consumption in versus those produced in China (a,e,i), South Korea (b,f,j), Japan (c,g,k), and Others (d,h,l). Scales are different for each column.



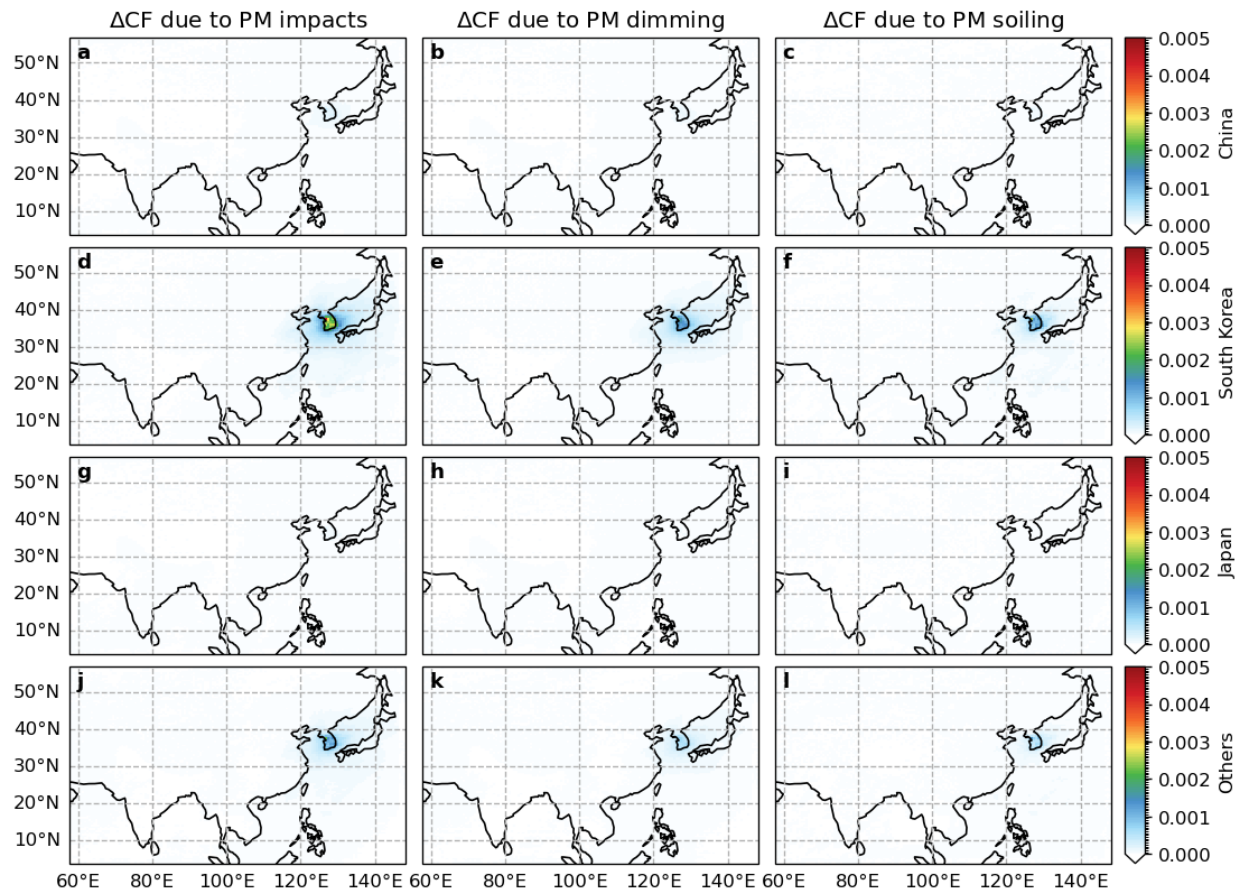
Supplementary Figure 2: The differences in annual mean PV efficiency losses due to deposited versus atmospheric PM associated with emissions produced in (a-d) and induced by consumption (e-h) in China (a,e), South Korea (b,f), Japan (c,g), and Others (d,h). Scales are different for each column.



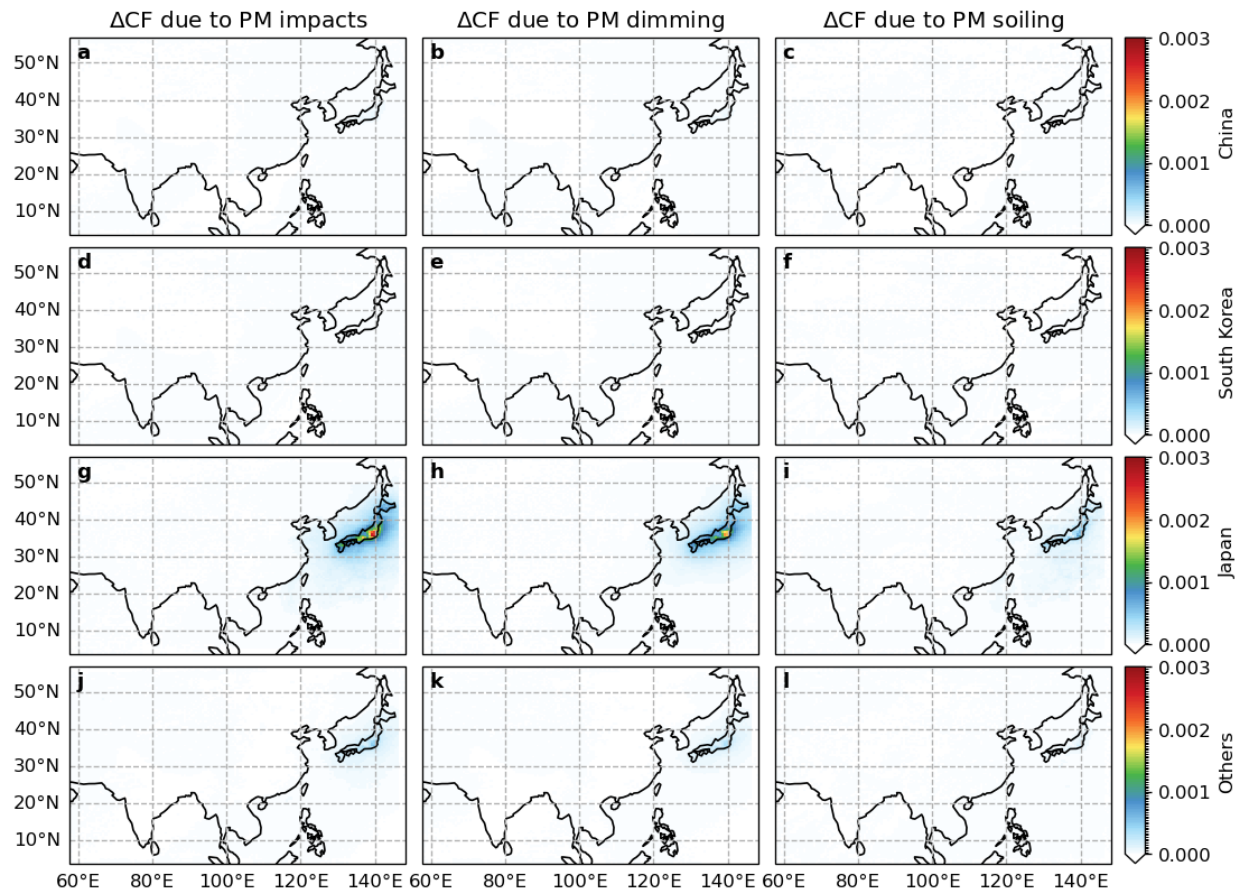
Supplementary Figure 3: The paired t–tests for the differences between consumption–based and production–based results of the source-receptor relationship of SEYGs due to PM pollution (**a**), including PM dimming (**b**) and soiling (**c**), among China, South Korea, and Japan. These statistical significance tests are conducted using the facility–level SEYGs data collected from each of the countries in each of the scenarios. T–statistics with associated p–values less than the significance level $\alpha = 0.01$ are marked with two asterisks (**), and it is observed that the differences between consumption-based and production-based results are all statistically significant.



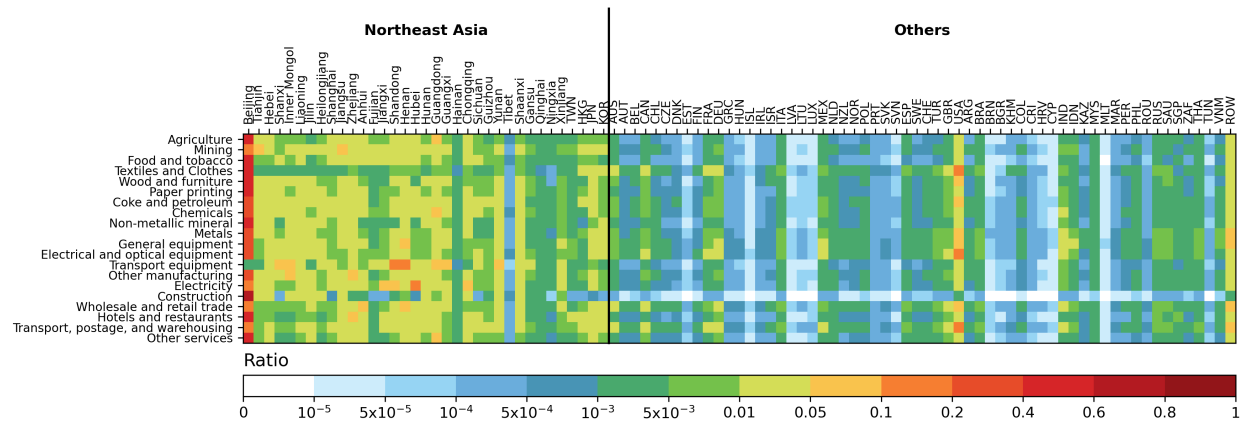
Supplementary Figure 4: Geographical distribution of annual mean losses of PV efficiency (ΔCFs) of OAT panels due to PM pollution (a,d,g,j), including PM dimming (b,e,h,k) and soiling (c,f,i,l), associated with emissions produced in China linked to consumption in China (a-c), South Korea (d-f), Japan (g-i), and elsewhere globally (j-l).



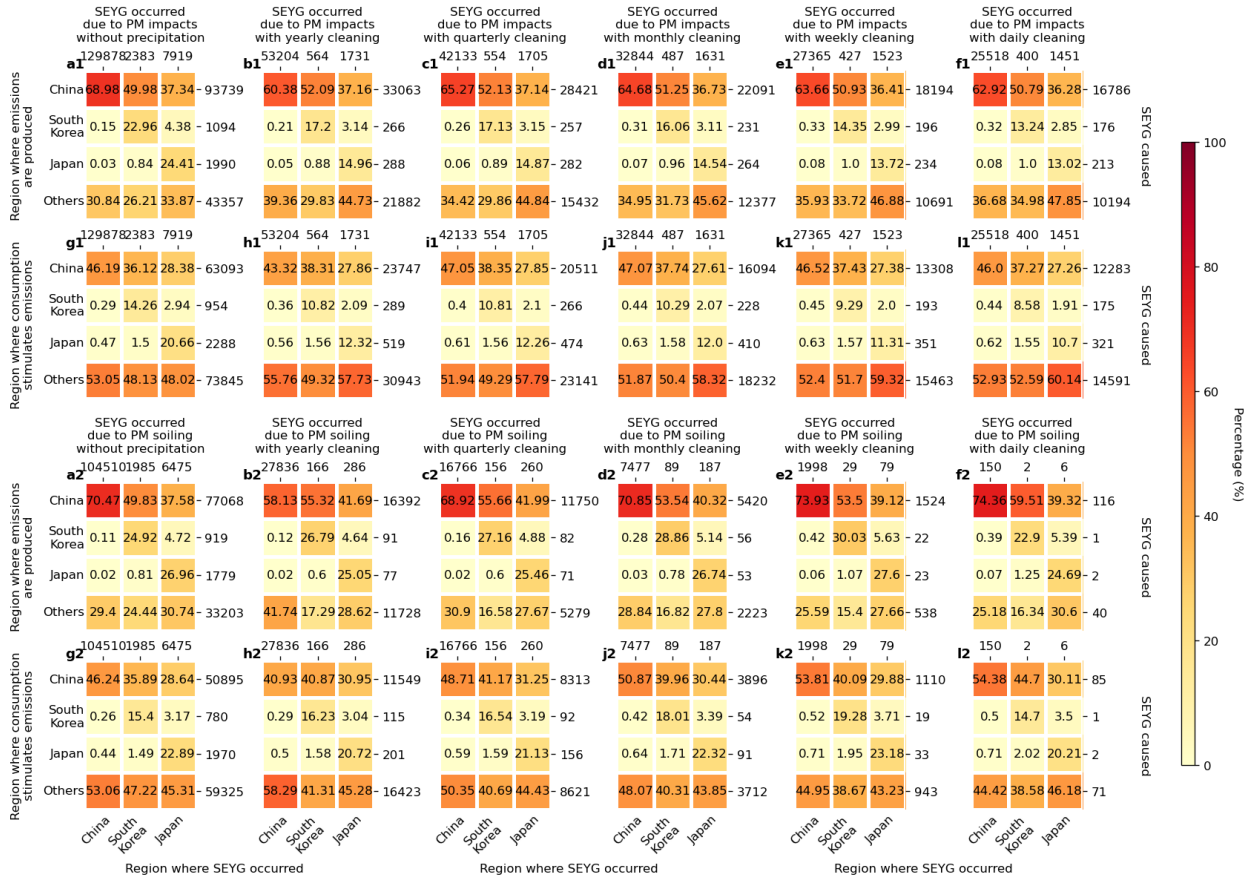
Supplementary Figure 5: Geographical distribution of annual mean losses of PV efficiency (ΔCFs) of OAT panels due to PM pollution (a-d-g-j), including PM dimming (b-e-h-k) and soiling (c-f-i-l), associated with emissions produced in South Korea linked to consumption in China (a-c), South Korea (d-f), Japan (g-i), and elsewhere globally (j-l).



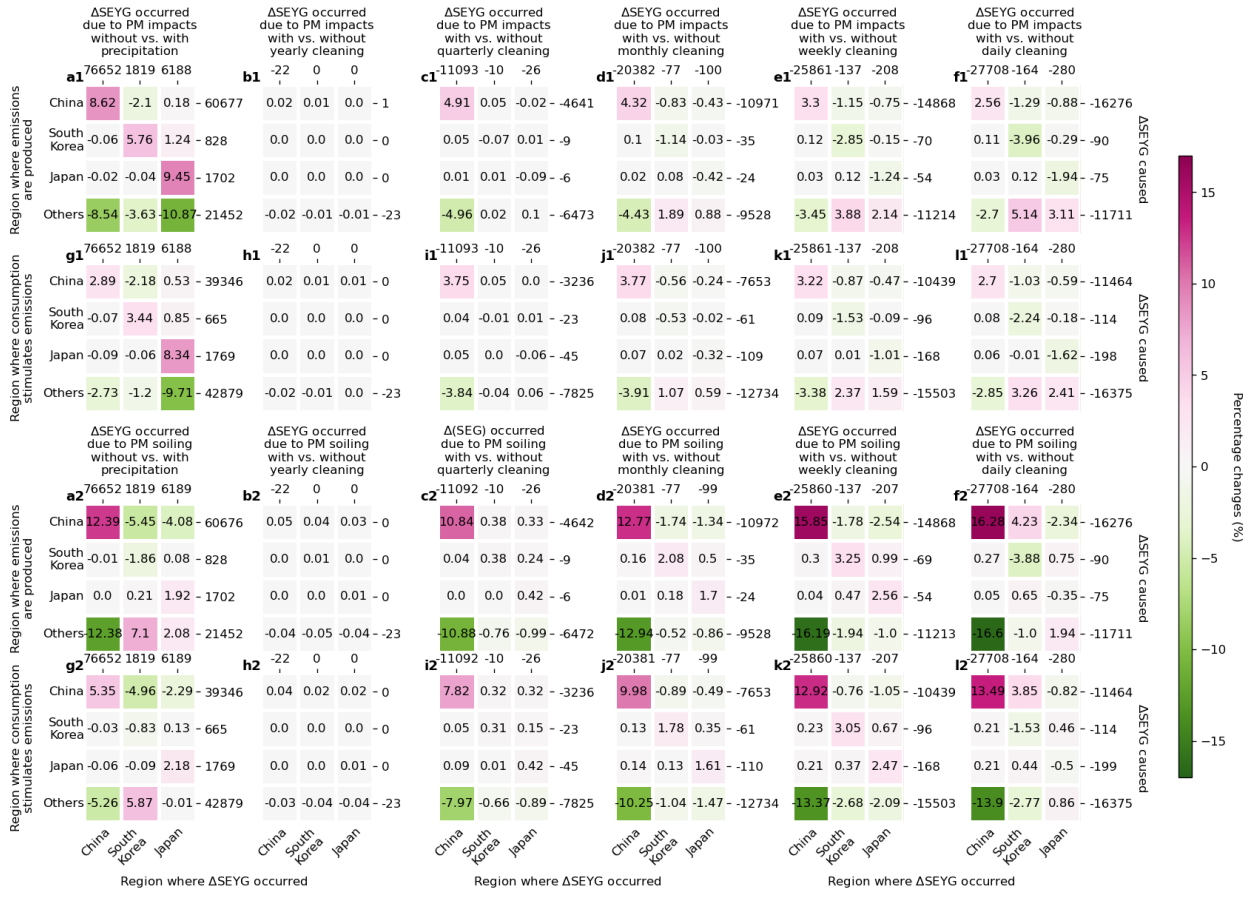
Supplementary Figure 6: Geographical distribution of annual mean losses of PV efficiency (ΔCFs) of OAT panels due to PM pollution (a-d-g-j), including PM dimming (b-e-h-k) and soiling (c-f-i-l), associated with emissions produced in Japan linked to consumption in China (a-c), South Korea (d-f), Japan (g-i), and elsewhere globally (j-l).



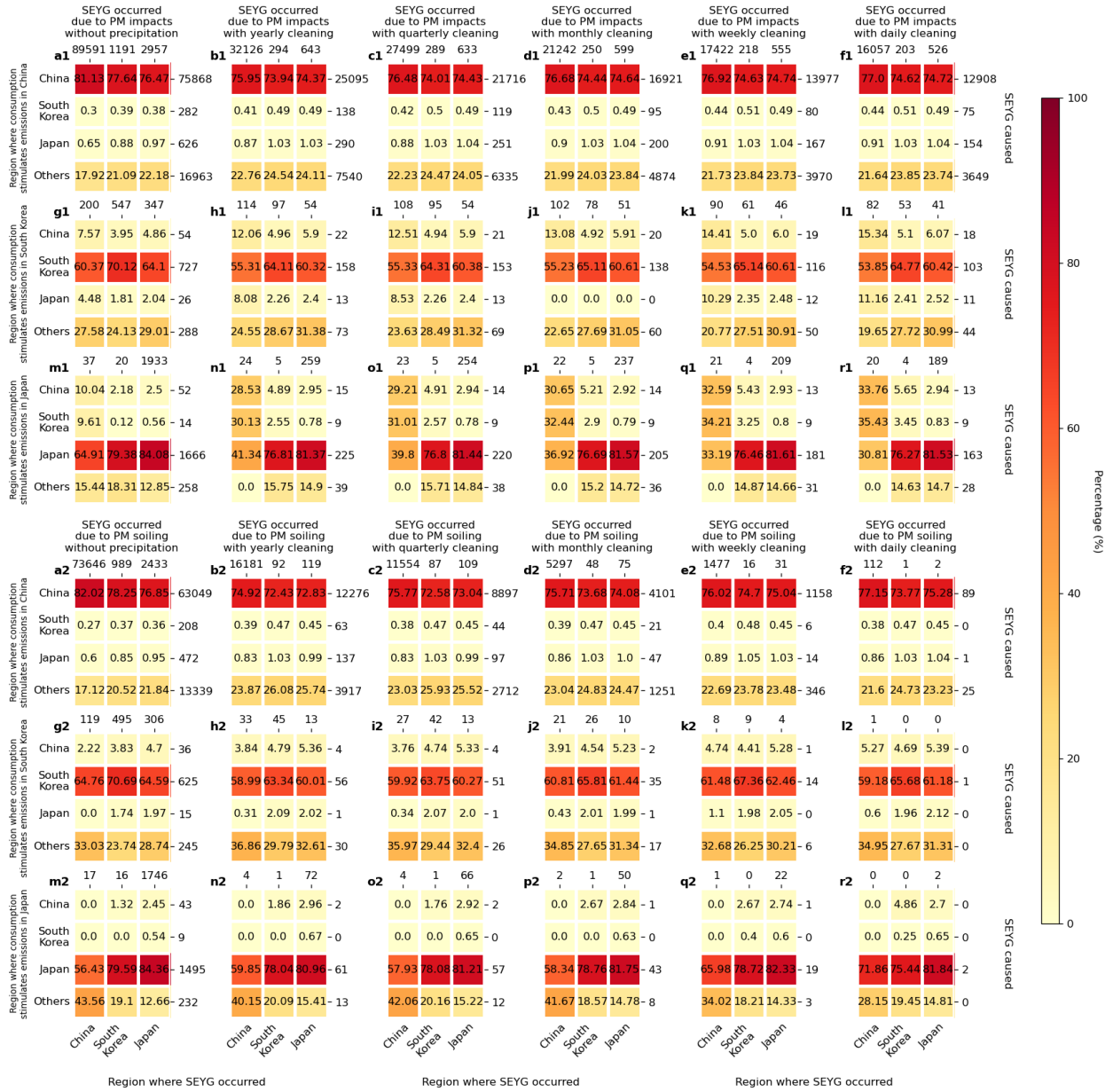
Supplementary Figure 7: Fraction of production of Beijing, China in each MRIO sector (from top to bottom) linked to consumption within Beijing itself and in other regions (from left to right).



Supplementary Figure 8: Contributions from source countrys' production— (a1-f1,a2-f2) and consumption–related (g1-l1,g2-l2) emissions to receptor countrys' SEYGs due to PM pollution (a1-l1) and its soiling (a2-l2) when excluding precipitation (a1,g1,a2,g2) and including panel cleaning on a yearly (b1,h1,b2,h2), quarterly (c1,i1,c2,i2), monthly (d1,j1,d2,j2), weekly (e1,k1,e2,l2), and daily (f1,l1,f2,l2) basis.



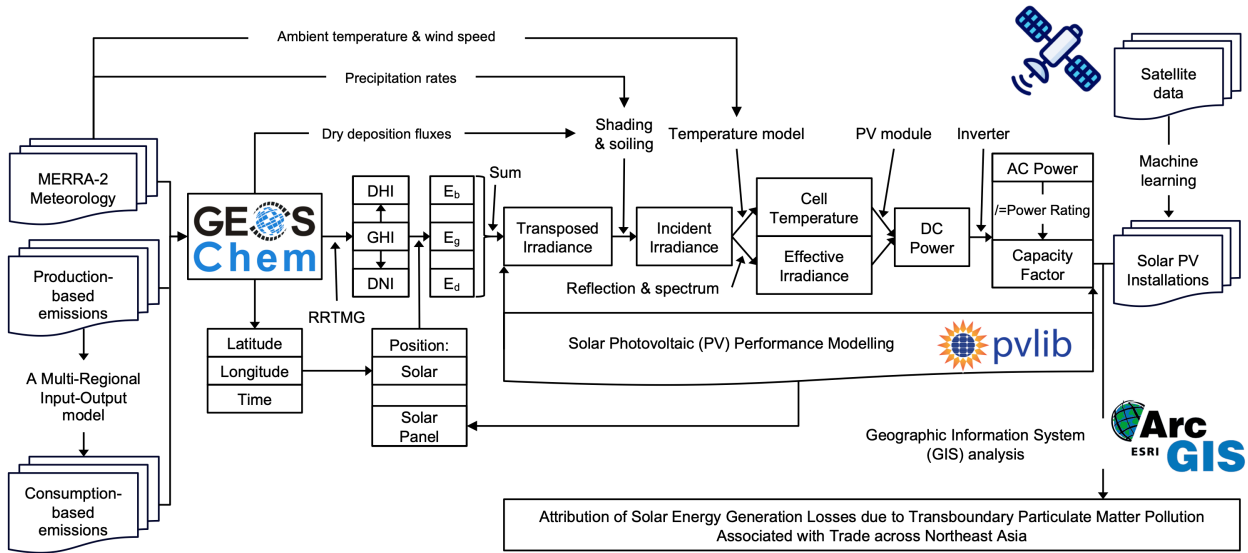
Supplementary Figure 9: The differences between the contributions from source countries' production- (**a1-f1,a2-f2**) and consumption-related (**g1-l1,g2-l2**) emissions to receptor countries' SEYGs due to PM pollution (**a1-l1**) and its soiling (**a2-l2**) when excluding precipitation (**a1,g1,a2,g2**) and including panel cleaning on a yearly (**b1,h1,b2,h2**), quarterly (**c1,i1,c2,i2**), monthly (**d1,j1,d2,j2**), weekly (**e1,k1,e2,j2**), and daily (**f1,l1,f2,l2**) basis, as compared to those contributions in the baseline scenario.



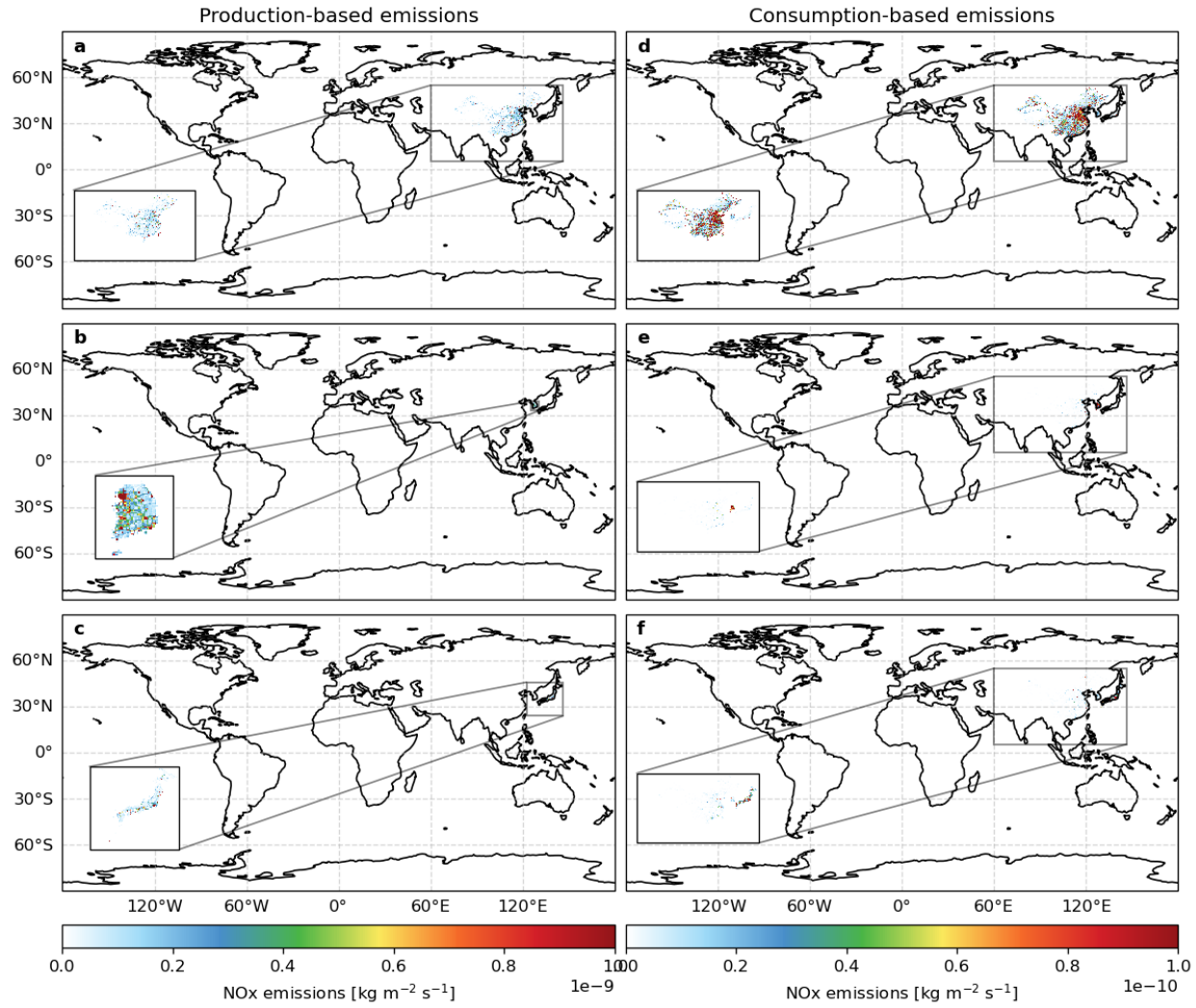
Supplementary Figure 10: Attribution of contributions of production-related emissions from China (**a1-f1**,**a2-f2**), South Korea (**g1-l1**,**g2-l2**), and Japan (**m1-r1**,**m2-r2**) to SEYGs in Northeast Asia due to PM pollution (**a1-r1**) and its soiling (**a2-r2**) to consumption in these countries and elsewhere globally when excluding precipitation (**a1,g1,m1,a2,g2,m2**) and including panel cleaning on a yearly (**b1,h1,n1,b2,h2,n2**), quarterly (**c1,i1,o1,c2,i2,o2**), monthly (**d1,j1,p1,d2,j2,p2**), weekly (**e1,k1,q1,e2,k2,q2**), and daily (**f1,l1,r1,f2,l2,r2**) basis.



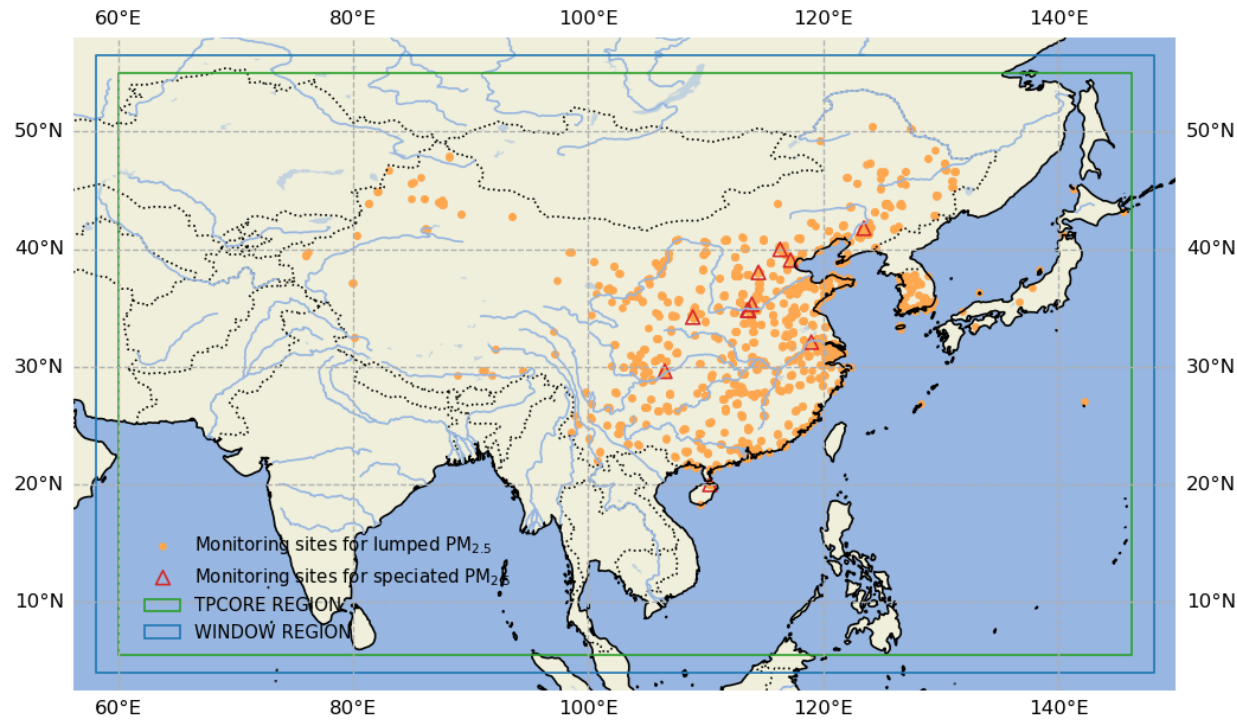
Supplementary Figure 11: The differences between the attribution of contributions of production-related emissions from China (**a1-f1,a2-f2**), South Korea (**g1-l1,g2-l2**), and Japan (**m1-r1,m2-r2**) to SEYGs in Northeast Asia due to PM pollution (**a1-r1**) and its soiling (**a2-r2**) to consumption in these countries and elsewhere globally when excluding precipitation (**a1,g1,m1,a2,g2,m2**) and including panel cleaning on a yearly (**b1,h1,n1,b2,h2,n2**), quarterly (**c1,i1,o1,c2,i2,o2**), monthly (**d1,j1,p1,d2,j2,p2**), weekly (**e1,k1,q1,e2,k2,q2**), and daily (**f1,l1,r1,f2,l2,r2**) basis, as compared to those attribution in the baseline scenario.



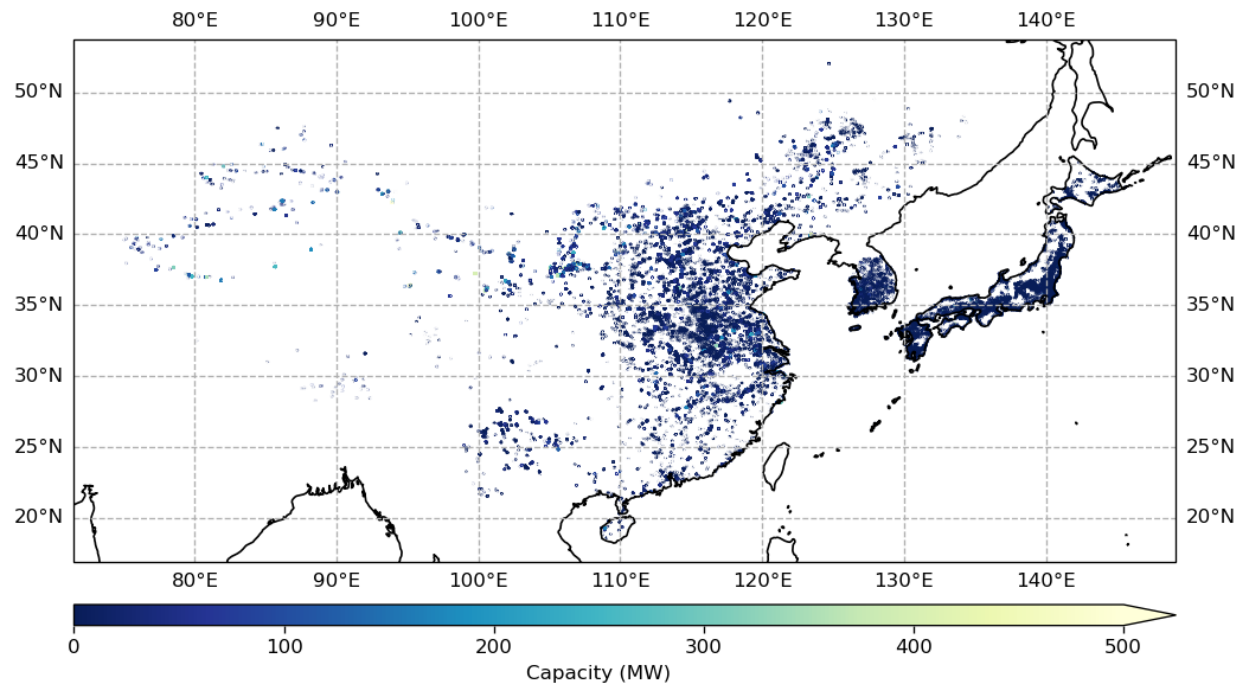
Supplementary Figure 12: Workflow to estimate and attribute SEYGs due to transboundary particulate matter pollution associated with trade across Northeast Asia. Full definitions of the acronyms include: 1) global horizontal irradiance (GHI) simulated from GEOS-Chem coupled with rapid radiative transfer model for GCMs (RRTMG), and it is subsequently decomposed to direct normal irradiance (DNI) and diffuse horizontal irradiance (DHI); 2) beam (E_b), ground-reflected (E_g), and sky-diffuse (E_d) components of transposed irradiance; and 3) direct (DC) and alternating (AC) current powers.



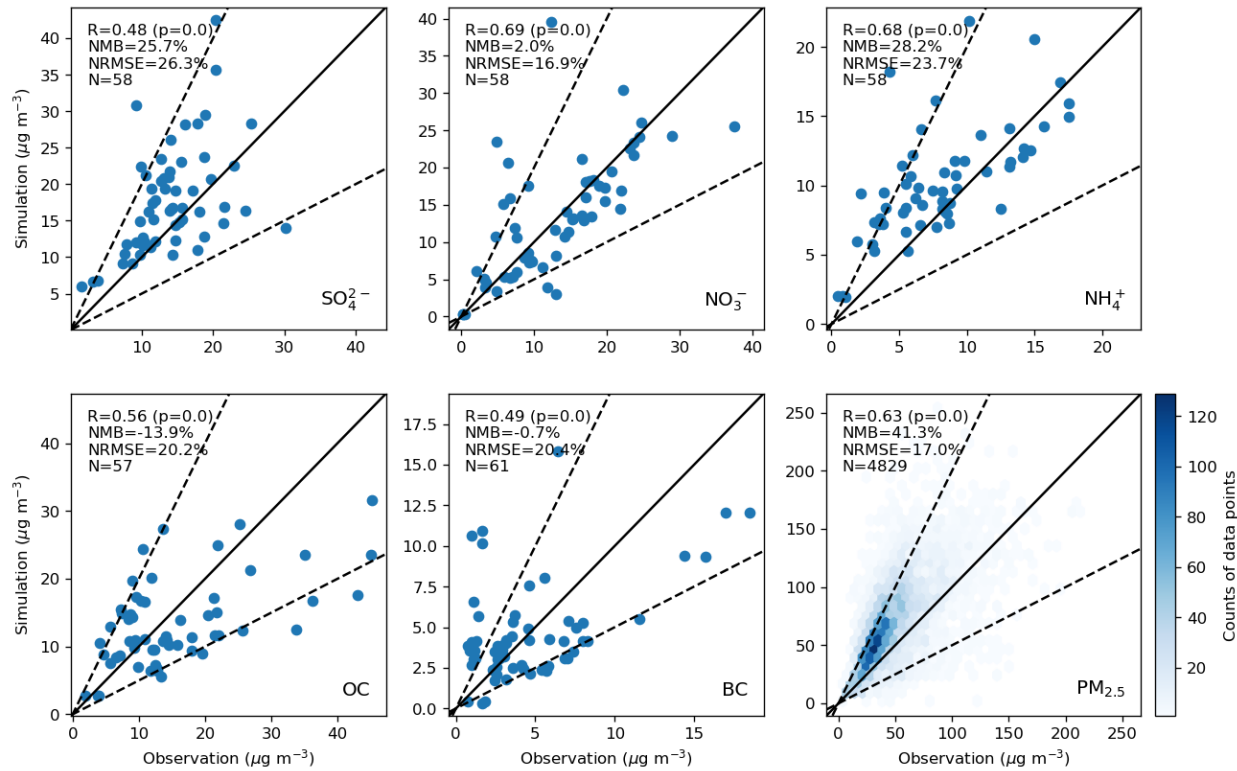
Supplementary Figure 13: Geographical distribution of annual mean production- (a-c) versus consumption-based (d-f) emission estimates in 2015, using NO_x as an illustration. The emissions produced in China, South Korea, and Japan are confined to the borders of these countries, as detailed in the insets. The emissions induced by consumption in these countries are lower in magnitude but more widely distributed across Northeast Asia, as highlighted in the insets. Scales are different for different columns.



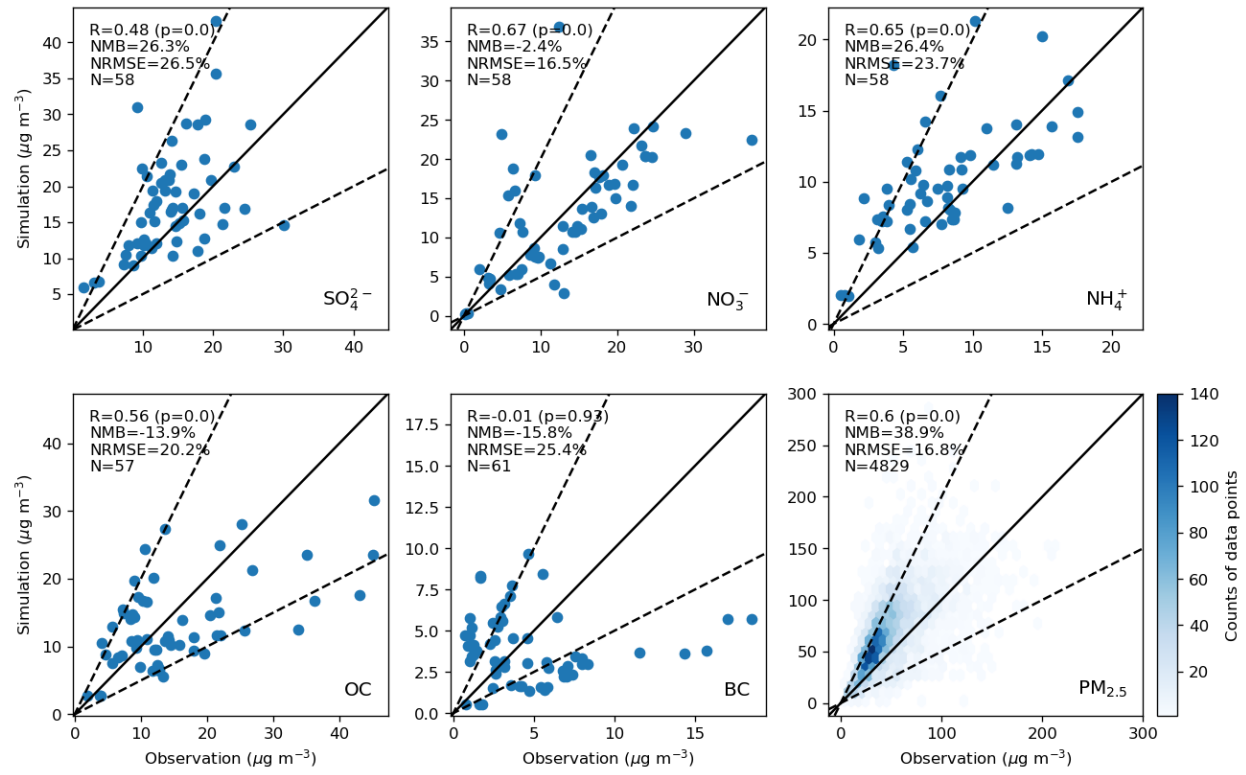
Supplementary Figure 14: The GEOS-Chem model domain used in this study overlaps with ground monitoring sites, indicated by orange dots (for lumped PM_{2.5}) and red triangles (for speciated PM_{2.5}). The ‘WINDOW REGION’ refers to the parent domain described with a $2^\circ \times 5^\circ$ resolution. The ‘TPCORE REGION’ refers to the nested domain described with a $0.5^\circ \times 0.625^\circ$ resolution. The region between them is where boundary conditions are applied.



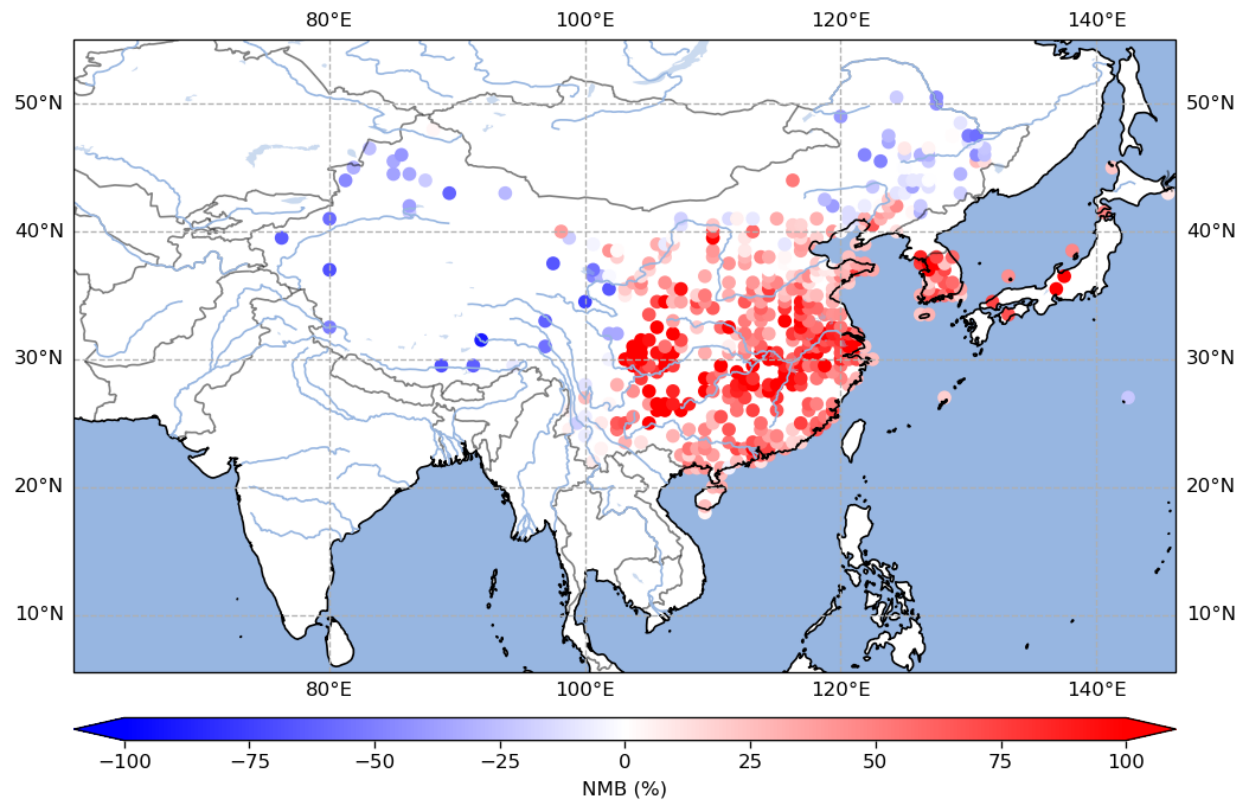
Supplementary Figure 15: Geographical distribution of solar PV installations across Northeast Asia, extracted and reproduced from ref 23. The colour of each polygon represents the estimated installed capacity of the detected and verified solar PV installations.



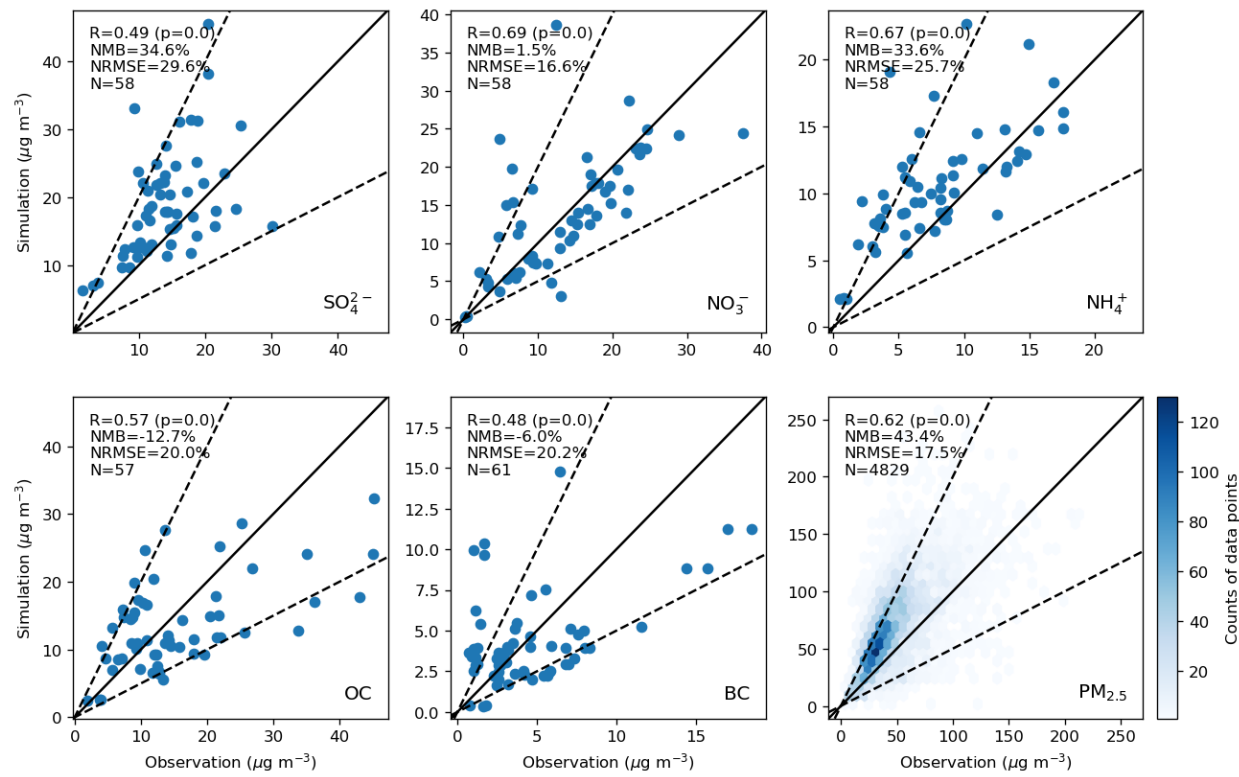
Supplementary Figure 16: Model evaluation results for the lumped $\text{PM}_{2.5}$ and its major chemical components, including sulfate (SO_4^{2-}), nitrate (NO_3^-), ammonium (NH_4^+), organic carbon (OC), and black carbon (BC) across Northeast Asia. The Pearson correlation coefficients (R), normalised mean bias (NMB), and normalised root mean squared error (NRMSE) are calculated for each species.



Supplementary Figure 17: Same as Figure 16 but without re-distributing black carbon emissions in EDGARv5.0 according to the spatial profile of the equivalent in the MIX Asian emission inventory.



Supplementary Figure 18: Site-scale model evaluation results for the lumped $\text{PM}_{2.5}$. The normalised mean bias (NMB) is calculated for each monitoring site.



Supplementary Figure 19: Same as Figure 16 but using EDGARv6.1 instead of EDGARv5.0.

References

- (1) Davis, S. J.; Caldeira, K. Consumption-based accounting of CO₂ emissions. *Proceedings of the national academy of sciences* **2010**, *107*, 5687–5692.
- (2) Davis, S. J.; Peters, G. P.; Caldeira, K. The supply chain of CO₂ emissions. *Proceedings of the National Academy of Sciences* **2011**, *108*, 18554–18559.
- (3) Lin, J.; Pan, D.; Davis, S. J.; Zhang, Q.; He, K.; Wang, C.; Streets, D. G.; Wuebbles, D. J.; Guan, D. Chinas international trade and air pollution in the United States. *Proceedings of the National Academy of Sciences* **2014**, *111*, 1736–1741.
- (4) Lin, J.; Tong, D.; Davis, S.; Ni, R.; Tan, X.; Pan, D.; Zhao, H.; Lu, Z.; Streets, D.; Feng, T.; others Global climate forcing of aerosols embodied in international trade. *Nature Geoscience* **2016**, *9*, 790–794.
- (5) Zhang, Q.; Jiang, X.; Tong, D.; Davis, S. J.; Zhao, H.; Geng, G.; Feng, T.; Zheng, B.; Lu, Z.; Streets, D. G.; others Transboundary health impacts of transported global air pollution and international trade. *Nature* **2017**, *543*, 705–709.
- (6) Crippa, M.; Guizzardi, D.; Muntean, M.; Schaaf, E.; Oreggioni, G. EDGAR v5.0 Global Air Pollutant Emissions. 2019; <http://data.europa.eu/89h/377801af-b094-4943-8fdc-f79a7c0c2d19>, Dataset.
- (7) Monforti Ferrario, F.; Crippa, M.; Guizzardi, D.; Muntean, M.; Schaaf, E.; Banja, M.; Pagani, F.; Solazzo, E. EDGAR v6.1 Global Air Pollutant Emissions. 2022; <http://data.europa.eu/89h/df521e05-6a3b-461c-965a-b703fb62313e>, Dataset.
- (8) Crippa, M.; Guizzardi, D.; Pagani, F.; Banja, M.; Muntean, M.; Schaaf, E.; Becker, W.; Monforti Ferrario, F.; Quadrelli, R.; Risquez Martin, A.; Grassi, G.; Rossi, S.; Brando De Melo, J.; Jacome Felix Oom, D.; Branco, A.; San-Miguel, J.; Vignati, E. EDGAR v8.1 Global Air Pollutant Emissions. 2024; <http://data.europa.eu/89h/a3af16e4-21ac-420a-b98c-b78a9b7723be>, Dataset.
- (9) Huang, G.; Brook, R.; Crippa, M.; Janssens-Maenhout, G.; Schieberle, C.; Dore, C.; Guizzardi, D.; Muntean, M.; Schaaf, E.; Friedrich, R. Speciation of anthropogenic emissions of non-methane volatile organic compounds: a global gridded data set for 1970–2012. *Atmospheric Chemistry and Physics* **2017**, *17*, 7683–7701.
- (10) Zheng, H.; Bai, Y.; Wei, W.; Meng, J.; Zhang, Z.; Song, M.; Guan, D. Chinese provincial multi-regional input-output database for 2012, 2015, and 2017. *Scientific data* **2021**, *8*, 244.
- (11) OECD OECD Inter-Country Input–Output (ICIO) Tables, 2018 edition. 2018; [https://data-explorer.oecd.org/vis?tenant=archive&df\[ds\]=DisseminateArchiveDMZ&df\[id\]=DF_IOTSI4_2018&df\[ag\]=OECD&dq=...&lom=LASTNPERIODS&lo=5&to\[TIME_PERIOD\]=false](https://data-explorer.oecd.org/vis?tenant=archive&df[ds]=DisseminateArchiveDMZ&df[id]=DF_IOTSI4_2018&df[ag]=OECD&dq=...&lom=LASTNPERIODS&lo=5&to[TIME_PERIOD]=false).

- (12) Bey, I.; Jacob, D. J.; Yantosca, R. M.; Logan, J. A.; Field, B. D.; Fiore, A. M.; Li, Q.; Liu, H. Y.; Mickley, L. J.; Schultz, M. G. Global modeling of tropospheric chemistry with assimilated meteorology: Model description and evaluation. *Journal of Geophysical Research: Atmospheres* **2001**, *106*, 23073–23095.
- (13) Heald, C.; Ridley, D.; Kroll, J.; Barrett, S.; Cady-Pereira, K.; Alvarado, M.; Holmes, C. Contrasting the direct radiative effect and direct radiative forcing of aerosols. *Atmospheric Chemistry and Physics* **2014**, *14*, 5513–5527.
- (14) Liu, J.; Yao, F.; Chen, H.; Zhao, H. Quantifying the mutual contributions of PM_{2.5} pollution and associated population exposure and premature deaths among China, South Korea, and Japan: A dual perspective and an interdisciplinary approach. 2024; <https://feiyao-edinburgh.github.io/files/PDF/liu2024quantifying.pdf>, In review.
- (15) Gelaro, R.; McCarty, W.; Suárez, M. J.; Todling, R.; Molod, A.; Takacs, L.; Randles, C. A.; Darmenov, A.; Bosilovich, M. G.; Reichle, R.; others The modern-era retrospective analysis for research and applications, version 2 (MERRA-2). *Journal of climate* **2017**, *30*, 5419–5454.
- (16) Yao, F.; Palmer, P. I. Source Sector Mitigation of Solar Energy Generation Losses Attributable to Particulate Matter Pollution. *Environmental Science & Technology* **2022**, *56*, 8619–8628.
- (17) Erbs, D.; Klein, S.; Duffie, J. Estimation of the diffuse radiation fraction for hourly, daily and monthly-average global radiation. *Solar energy* **1982**, *28*, 293–302.
- (18) Loutzenhiser, P. G.; Manz, H.; Felsmann, C.; Strachan, P.; Frank, T.; Maxwell, G. Empirical validation of models to compute solar irradiance on inclined surfaces for building energy simulation. *Solar Energy* **2007**, *81*, 254–267.
- (19) Bergin, M. H.; Ghoroi, C.; Dixit, D.; Schauer, J. J.; Shindell, D. T. Large reductions in solar energy production due to dust and particulate air pollution. *Environmental Science & Technology Letters* **2017**, *4*, 339–344.
- (20) Li, X.; Mauzerall, D. L.; Bergin, M. H. Global reduction of solar power generation efficiency due to aerosols and panel soiling. *Nature Sustainability* **2020**, *3*, 720–727.
- (21) Holmgren, W. F.; Hansen, C. W.; Mikofski, M. A. pvlib python: A python package for modeling solar energy systems. *Journal of Open Source Software* **2018**, *3*, 884.
- (22) Li, X.; Wagner, F.; Peng, W.; Yang, J.; Mauzerall, D. L. Reduction of solar photovoltaic resources due to air pollution in China. *Proceedings of the National Academy of Sciences* **2017**, *114*, 11867–11872.
- (23) Kruitwagen, L.; Story, K.; Friedrich, J.; Byers, L.; Skillman, S.; Hepburn, C. A global inventory of photovoltaic solar energy generating units. *Nature* **2021**, *598*, 604–610.

- (24) Sweerts, B.; Pfenninger, S.; Yang, S.; Folini, D.; Van der Zwaan, B.; Wild, M. Estimation of losses in solar energy production from air pollution in China since 1960 using surface radiation data. *Nature Energy* **2019**, *4*, 657–663.
- (25) Hammer, M. S.; van Donkelaar, A.; Li, C.; Lyapustin, A.; Sayer, A. M.; Hsu, N. C.; Levy, R. C.; Garay, M. J.; Kalashnikova, O. V.; Kahn, R. A.; others Global estimates and long-term trends of fine particulate matter concentrations (1998–2018). *Environmental Science & Technology* **2020**, *54*, 7879–7890.
- (26) Li, M.; Zhang, Q.; Kurokawa, J.-i.; Woo, J.-H.; He, K.; Lu, Z.; Ohara, T.; Song, Y.; Streets, D. G.; Carmichael, G. R.; others MIX: a mosaic Asian anthropogenic emission inventory under the international collaboration framework of the MICS-Asia and HTAP. *Atmospheric Chemistry and Physics* **2017**, *17*, 935–963.